Lithospheric structuration onshore-offshore of the Sergipe-Alagoas passive margin, NE Brazil, based on wide-angle seismic data

J.M. Pinheiro, P. Schnürle, M. Evain, A. Afilhado, F. Gallais, F. Klingelhoefer, A. Loureiro, R. Fuck, J. Soares, A. Cupertino, et al.

Journal of South American Earth Sciences
December 2018, Volume 88, Pages 649-672
https://doi.org/10.1016/j.jsames.2018.09.015
https://archimer.ifremer.fr/doc/00461/57263/

Lithospheric structuration onshore-offshore of the Sergipe-Alagoas passive margin, NE Brazil, based on wide-angle seismic data ☆

Pinheiro Joao Marcelo [1,*], Schnurle Philippe [1], Evain Mikael [1], Afilhado A. [2], Gallais Flora [1], Klingelhoefer Frauke [1], Loureiro Afonso [3], Fuck R. [4], Soares J. [4], Cupertino J.A. [5], Viana A. [5], Rabineau Marina [6], Baltzer Agnes [7], Benabdellouahed Massinissa [6], Dias N. [2,3], Moulin Maryline [1], Aslanian Daniel [1], Morvan Laetitia [8], Mazé Jean-Pierre [8], Pierre Delphine [8], Roudaut-Pitel M. [8], Rio I. [9], Alves D. [9], Barros Junior P. [11], Biari Youssef [8], Corela C. [9], Crozon Jacques [8], Duarte J.L. [9], Ducatel Cecile [8], Falcão C. [11], Fernagu Philippe [8], Le Piver David [8], Mokeddem Zohra [10], Pelleau Pascal [8], Rigoti C. [11], Roest Walter [8], Roudaut Mickael [8]

[1] Institut Français de Recherche pour l'Exploitation de la MER, IFREMER, REM/GM, Centre de Brest, 29280, Plouzané, France
[2] Instituto Superior de Engenharia de Lisboa, ISEL, Instituto Politécnico de Lisboa, R. Conselheiro Emídio Navarro, 1959-007, Lisbon, Portugal
[3] Instituto Dom Luiz, Faculdade de Ciências, Universidade de Lisboa, Campo Grande, Ed. C1, Piso 1, 1749-016, Lisbon, Portugal
[4] Instituto de Geociências, Universidade de Brasília, Campus Darcy Ribeiro, 70910-900, Brasilia, Brazil
[5] Petrobras, Cenpes Research Center, Rio de Janeiro, Brazil
[6] Laboratoire Géosciences Océan, UMR6538, Université de Bretagne Occidentale, Place Nicolas Copernic, 29280, Plouzané, France
[7] Géolittomer, LETG UMR 6554-CNRS, Institut de Géographie et d'Aménagement Régional de l'Université de Nantes, Campus Tertre, BP 81227, 44312, Nantes, CEDEX 3, France
[8] Institut Français de Recherche pour l'Exploitation de la MER, IFREMER, REM/GM, Centre de Brest, 29280, Plouzané, France
[9] Instituto Dom Luiz, Faculdade de Ciências, Universidade de Lisboa, Campo Grande, Ed. C1, Piso 1, 1749-016, Lisbon, Portugal
[10] Laboratoire Géosciences Océan, UMR6538, Université de Bretagne Occidentale, Place Nicolas Copernic, 29280, Plouzané, France
[11] Géolittomer, LETG UMR 6554-CNRS, Institut de Géographie et d'Aménagement Régional de l'Université de Nantes, Campus Tertre, BP 81227, 44312, Nantes, CEDEX 3, France

* Corresponding author : Joao Marcelo Pinheiro, email address : jmpgeo@gmail.com

Abstract :

The structure and nature of the crust underlying the Camamu-Almada-Jequitinhonha-Sergipe-Alagoas basins System, in the NE Brazilian margin, were investigated based on the interpretation of 12 wide-angle seismic profiles acquired during the SALSA (Sergipe ALagoas Seismic Acquisition) experiment in 2014. In this work, we present two 220-km-long NW-SE combined wide-angle and reflection seismic profiles, SL 01 and SL 02, that have been acquired using 15 ocean-bottom-seismometers along each profile, offshore the southern part of the Sergipe Alagoas Basin (SAB), north of the Vaza-Barris Transfer zone. The SL 02 has a 150-km long inland continuation with 20 land-seismic-stations until the Sergipano Fold Belt (SFB). Wide-angle seismic forward modeling allows us to precisely divide the crust in three domains: beneath the continental shelf, a ~100 km wide necking zone is imaged where the continental crust thins from ~35 km on the Unthinned Continental Domain, which displays a three-layered crust structure, to less than 8 km on the Oceanic Crust Domain. In the necking zone, the upper and the middle layers thin dramatically and almost disappear, while the Moho discontinuity shows clear PmPs. The Continental-Oceanic Crust Boundary (COB) is located at ~80 km from the coastline and is marked by intracrustal seismic reflectors and changes in the seismic velocity, showing a sharp transition. On profile SL02, the oceanic crust is perturbed by a volcanic edifice together with an anomalous velocity zone underneath the area.

Highlights

► Sergipe Alagoas Basin passive margin modeling. ► Wide-angle refraction seismic integrated with Multi-Channel reflection seismic data. ► Location of the Continental- Oceanic crust boundary. ► Lithospheric structuration and segmentation of Brazil's margin in Central Atlantic.

Keywords : South Atlantic Ocean, NE Brazil, Sergipe-Alagoas Basin, Passive Margins, Wide-angle refraction seismics, Crustal structure, Tectonic Inheritance.

☆ We would like to thank two anonymous reviewers and the editor Dr. F. Audemard, who helped to improve significantly this manuscript.

Introduction

Understanding the processes that led to the breakup of West Gondwana (Figure 1A) and the formation of the south Atlantic Margins are still not fully achieved. The North – East Brazilian margins, which are very segmented margins, in various structural and inheritance contexts, where the aborted Recôncavo - Tucano - Jatoba rift system connects with the NS Jequitinhonha - Camamu-Almada and NE-SW Jacuípe - Sergipe-Alagoas rift systems are a strategic area to study the influence of the tectonic inheritance on margin's formation. The connection between the three system forms the Camamu triple junction. The SALSA experiment, conducted in 2014 by the Department of Marine Geosciences (IFREMER: Institut Français de Recherche pour l'Exploitation de la MER, France) and PETROBRAS (Brazil), in collaboration with the Laboratory of Oceanic Domain (IUEM: Institut Universitaire et Européen de la Mer, France), the Faculdade de Ciências da Universidade de Lisboa (IDL, Portugal) and the Universidade de Brasilia (Brazil), is aimed at constraining the crustal structure, the segmentation and the geodynamical setting of the Jequitinhonha-Almada-Camamu-Jacuípe-Alagoas-Sergipe margin segments.

In the year 2000's high quality seismic profiles from ION-GXT were acquired off Brazil's coast, and a few of these profiles have been published, particularly in the Brazilian southeastern margin (e.g., Henry *et al.*, 2009; Kumar *et al.*, 2012). The location of the SALSA profiles follows the location of some of the ION-GXT profiles. Seismic shots, Multi-Channel Seismic (MCS) acquisition and Ocean Bottom Seismometers (OBS) deployments were performed by the French R/V L'Atalante (IFREMER) along twelve profiles (Figure 1B). Among them, five were extended onshore by Land Seismic Stations (LSS). Here, we present the results on P-wave velocity models, based on the combined interpretation of multi-channel and wide-angle seismic data, of two profiles imaging the Sergipe-Alagoas basin (SAB), located in the northern part of the experiment, north to the Vaza-Barris transfer zone (Figures 1C and 2). The remaining basins studied during the SALSA project (Camamu (Loureiro *et al.*, 2018), Jacuípe, Tucano and Sergipe-Alagoas basins) will be discussed in companion papers.

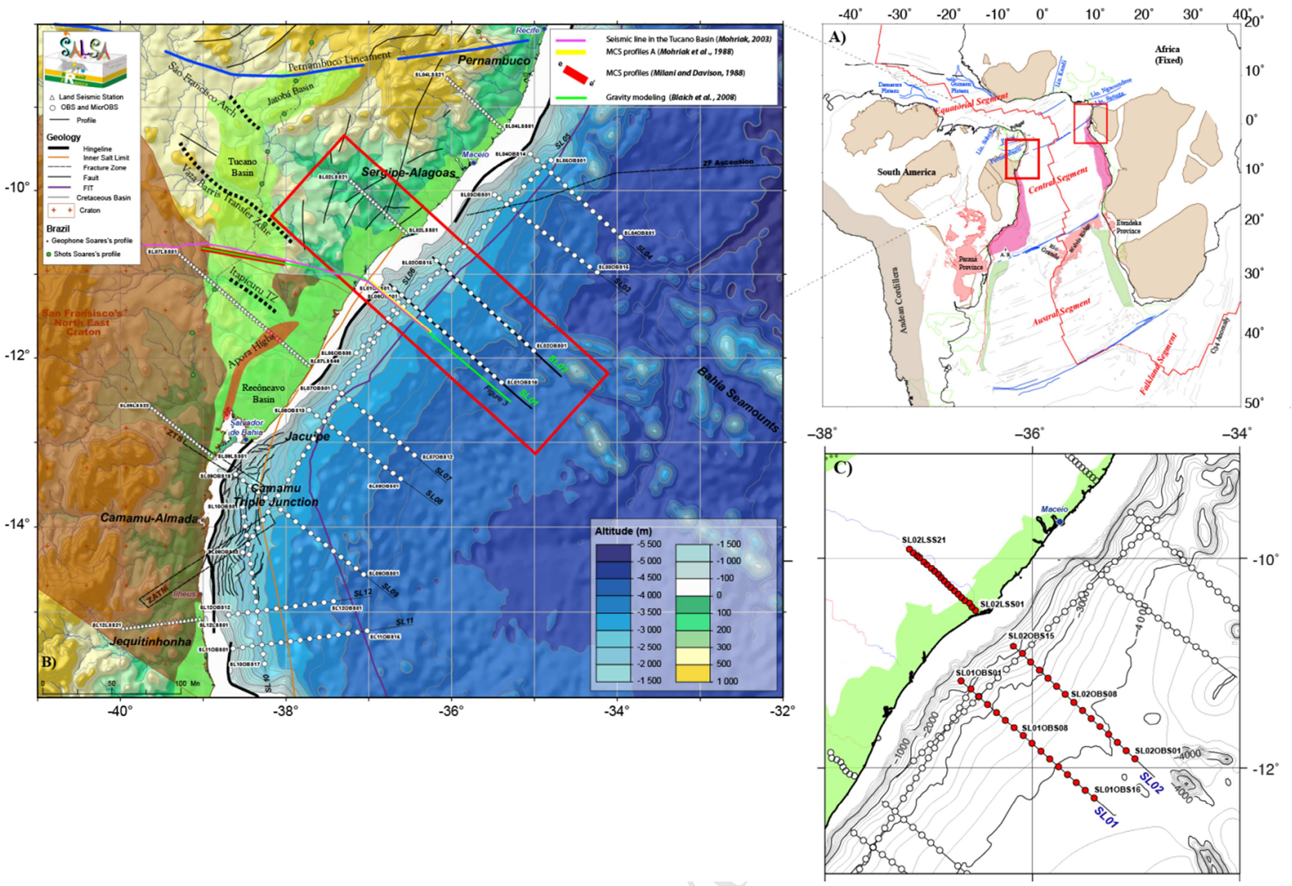

Figure 1: Location of profiles of the SALSA experiment: A) General reconstruction map at Chron C34 of studied area and conjugate margin (Moulin et al., 2010). B) Bathymetry and topography on land (IHO-IOC GEBCO, 2014). Ocean Bottom Seismometers (OBSs) are marked by white dots, MCS profiles by thick black lines, land-stations by white triangles. The SL01 and SL02 profiles are highlighted by red rectangle. The color lines represent the location of profiles already published in this area. Dashed black line denotes main transfer zones (Blaich et al., 2008). Green area indicates the Recôncavo-Tucano-Jatoba (RTJ) basins (Bizzi et al., 2003). Brown area indicates the limits of the Sao Francisco Craton, adapted from Hasui (2012). TMAZ: Taipus-Mirim Accommodation Zone. Note that Bahia Seamounts are characterized by an elongated NW-SE direction. C) Bathymetry (IHO-IOC GEBCO, 2014) around the profiles discussed in the present paper.

Geological Setting

Whilst in Albian time the central part of the South Atlantic presented the first oceanic crust, the Equatorial Atlantic Ocean was only starting to open, as the last stage of the breakup of the Atlantic Ocean, allowing the definitive water connection between the Central Atlantic and the South Atlantic oceans (Moulin *et al.*, 2010). From the Potiguar Basin to the north to the Camamu triple junction to the south (figure 1A), this area represents a buffer zone between these two different geodynamical settings (Conceiçao and Zalan, 1998; Moulin *et al.*, 2010).

This buffer zone is characterized by a SW-NE elongated margin, oblique respect to the main direction of the Fracture zones of the central segment of the South Atlantic Ocean. Onshore the presence of a failed N-S and E-W rift: the Recôncavo-Tucano-Jatoba rift, marks the limit of the Triangle-shaped Tucano Microplate, which rotated counterclockwise (Szatmari *et al.*, 1999; Moulin *et al.*, 2010) during the South Atlantic opening. The Sergipe Alagoas Basin (SAB) is situated in the middle of the eastern branch of this triangle, to the north of the Vaza-Barris Fault, which marks the boundary between the Sergipe basin and Jacuipe basin depocenters. It is in the east of the Sergipano Fold Belt (SFB) and south of the Pernambuco lineament, which are geological structures associated with the tectonic development of NE Brazil (Figure 2), inherited from the Neoproterozoic Brasiliano Orogeny (Davison *et al*., 1995). The role of the Vaza-Barris transfer zone, is not yet completely understood, but it plays a significant role in the actual framework of the Brazilian margin, as it divides the Tucano basin and produces a flip in the location of its depocenters. Stratigraphically, the SAB is one of the few basins that presents Paleozoic to Jurassic/Early Cretaceous pre-rift sequences related to intracratonic subsidence and is the northern limit of the evaporite deposits (Cainelli and Mohriak, 1998).

Sediments in the SAB lie over the Proterozoic SFB (Figure 2). The SFB is located between the Pernambuco-Alagoas Massif and the São Francisco Craton (SFC) (Figures 1 and 2) with a triangular shape narrowing towards the west (Figure 2). The geological history of the SFB has been the subject of numerous studies (e.g. Almeida *et al.,* 1977; Davison and Santos, 1989; D'el-Rey Silva, 1999). Recently Oliveira *et al.* (2010), based on U–Pb SHRIMP (Sensitive High-Resolution Ion Microprobe) and detrital zircons ages from Carvalho *et al.* (2005), proposed that the evolution of the Sergipano Belt began with the breakup of a Palaeoproterozoic continent followed by development of a Mesoproterozoic (≈980–960 Ma) continental arc possibly on the margin of the Palaeoproterozoic Pernambuco-Alagoas Massif. The extension of this continental block resulted in a stretched margin, a passive margin on the southern edge of the Pernambuco-Alagoas Massif with a rift in between. A second passive margin was formed on the São Francisco Craton. Convergence of the Pernambuco-Alagoas Massif and the São Francisco Craton led to deformation in shelf sediments, build-up of a continental arc between 630 Ma and 620 Ma, and subsequent exhumation and erosion of the Pernambuco-Alagoas Block, led to deposition of the uppermost Pre-Cambrian clastic sediments (Oliveira *et al.,* 2010).

The SAB presents a complete rift stratigraphic record (Mohriak, 2003). The initial rift deposits records can be observed in the onshore part of the SAB. Gomes (2005), using well logs information with seismic data (Cainelli, 1992), had tracked continuous seismic horizons related to the base of the Calumbi Formation, which marks the beginning of the drift phase. Campos Neto *et al.* (2007) elaborated the Petrobras stratigraphic chart, following the lithostratigraphic classification proposed by Schaller (1970) and Feijó (1994).

Mohriak *et al.* (1995, 1998, 2000) and Mohriak (2003) interpreted the regional seismic section 238-RL-343 (Figures 1 and 3). This profile is perpendicular to the coast and hinge line and extends for about 110 km from the platform to the deep water-region of the SAB. He did an interpretation stratigraphically calibrated by exploration boreholes and structurally constrained by gravity modelling. The results of a deep geoseismic transect were also used by Blaich *et al.* (2008, 2011) to model the crust of the SAB in combination of new gravity data. From these past studies, we can assume some key elements:

- Mohriak *et al*. (1998) described a conspicuous array of strong undulated reflectors in the lower portion of the profile (Figure 3) forming an anticlinal structure that rises from the westernmost portion of the profile until the apex near the shelf-break and extends as a band of reflectors throughout most of the profile (Figure 3), from slope to deep basin. He suggested that they might correspond to intracrustal horizons that probably mark the transition from the lower crust to the upper mantle ultramafic rocks (Kemplerer *et al.*, 1986).
- Mohriak *et al*. (1998) observed some structures in the proximal deep-water basin that was interpreted as igneous bodies (Figure 3). One example is a plug interpreted as a post-rift volcanic intrusion close to the Continental Ocean Boundary (COB) (Figure 3). Bordering this plug, in the proximal side, there are packages of reflectors with a sigmoidal geometry, mostly dipping seawards, but also dipping landwards, that probably correspond to seaward-dipping-reflectors and landward dipping reflectors (SDRs and LDRs) (Figure 3), which were interpreted as formed by volcanic rocks extruded during early phases of spreading oceanic ridges (Mohriak *et al*., 1998). These magmatic features are usually associated with extensional processes and oceanic crust inception, and therefore post-date the rift-phase lithospheric extension associated with the break-up of Gondwana in the Early Cretaceous. On the base of this observations, Mohriak *et al.* (1995) suggested that the central segment of the South Atlantic African margins could also be considered as a volcanic margin such as the Norwegian margin (e.g. Eldholm *et al.*, 1989), the Greenland margin (e. g. Korenaga *et al.*, 2000), the Aden margin (Tard *et al.*, 1991) or the Namibia margin (Bauer *et al.*, 2000; Austin and Uchupi, 1982). However, Moulin *et al.* (2005) have quoted the differences between the 4 km thick SDRs layer lying on top of a 30km-thick igneous crust and extending over a lateral distance of 150km on the Greenland margin (Korenaga *et al.*, 2000) and this less than 20km wide and less than 3km thick SDRs described by Mohriak *et al.* (1995). They argued that if their thickness is similar, their lateral extensions are quite different and the same genetic process can hardly be attributed to both structures.
- Assuming a simple geologic model based in thinning of the crust with mantle rising from 35 km in the onshore region to about 25 km at the platform, and to about 20 km near the shelf edge, the gravity modelling for the Sergipe sub-basin and the Jacuipe Basin suggests a very rapid crustal thinning near the present-day shelf edge (Mohriak *et al.*, 1995, 1998). According to this modelling, the Moho topography gets more regular from slope to seawards with depths between 15 and 18 km across the COB (Figure 3).

- In addition to the rapid shallowing of the Moho and the presence of SDRs, the 2D gravity modeling of Blaich *et al.* (2008) required the introduction of a lower crustal high-density body in the proximal part of the gravimetric profile, in the necking zone, between 200 km and 300 km distance (Figure 4). For these authors this high-density body would indicate a volcanic margin character.
- The COB location was evaluated by this 2D gravity modelling (Blaich *et al.*, 2008) and illustrates also a Moho discontinuity that shallows very rapidly eastward of the depocenter, rising from 33 km to 18 km depth within a distance of about 70 km, not so different of the model proposed by Mohriak *et al*. (1998).

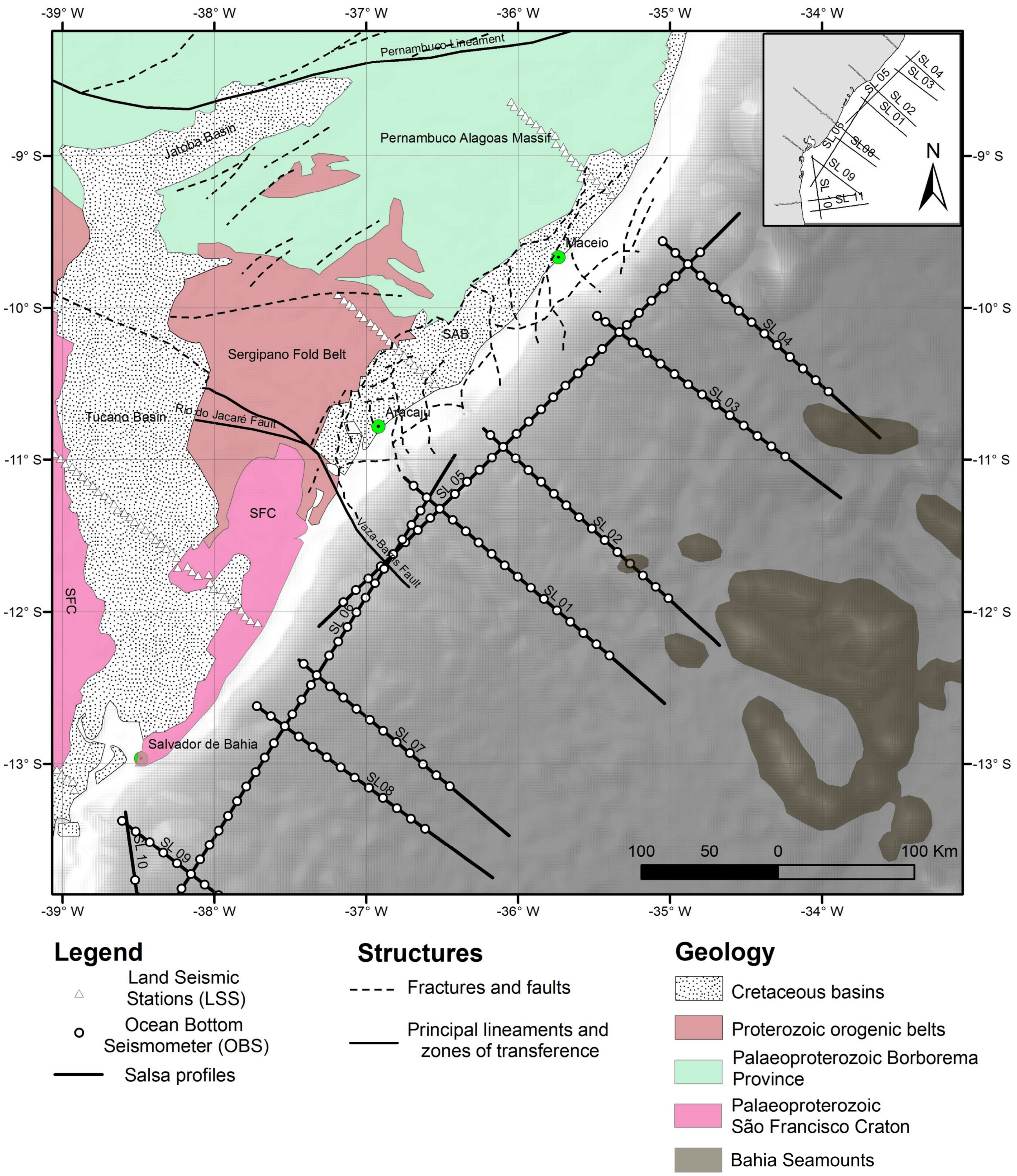

Figure 2. Geological Map of the Basin Sergipe-Alagoas and region around (modified from Lana, 1990,) with the SALSA profiles, the principal faults and fractures, and the geological features associated with the São Francisco Craton (SFC), the SFB and the Sergipe Alagoas Basin (SAB). Mercator projection.

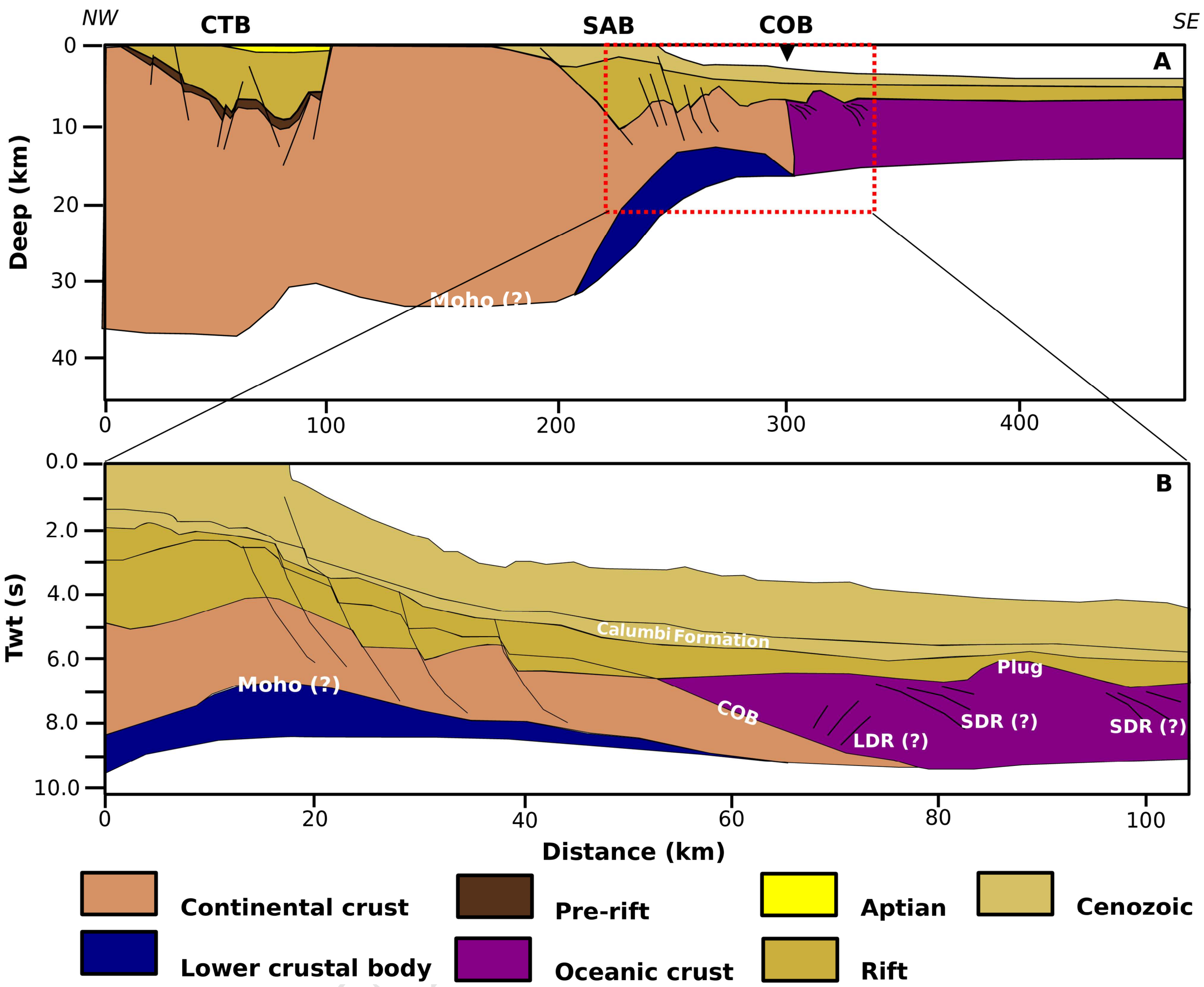

Figure 3: a) Gravity modelled transect in SAB modified from Blaich et al. (2008), represented by the blue line in figure 1. The red dotted square in the gravity model represents the location of the seismic profile 239-RL-343, the area inside the square was modelled based on seismic data and the rest on gravity data; b) Interpreted deep seismic profile 239-RL-343 by Mohriak et al. (1995, 1998, 2000), represented by the red line in figure 1. CTB, Central Tucano Basin; SAB, Sergipe Alagoas Basin; COB Continental-Oceanic Boundary; SDR, Seaward Dipping Reflectors; LDR, Landward Dipping Reflectors.

Data Processing and Modeling

The ION-GXT profiles are high quality reflection seismic profiles. However, the time-to-depth inversion made to transform the time data into depth data are not based on high-accuracy crustal P-wave velocities. The SALSA refraction seismic profiles were located following some ION-GXT profiles positions, allowing in the future an integration of more detailed crustal P-wave velocities obtained by wide-angle refraction data. During the SALSA experiment, Multi-Channel Seismic (MCS) acquired jointly with refraction data was processed using the Geocluster (CGG Veritas) software. The processing sequence was composed of geometry, wave-equation multiple attenuation, shot-gather predictive deconvolution, time variant band-pass filter, random multiple attenuation, normal move-out, CMP stack and post-stack FK time migration. A last step of seismic data processing is the pre-stack depth migration of the MCS data using the results of wide-angle seismic data modeling, followed by residual move-out analysis. This procedure uses both near-vertical and wide-angle seismic data sets to produce a depth seismic section, which images both the sedimentary crust as well as the basement. Furthermore, it allows to verify the accuracy of the wide-angle velocity model in the sedimentary sequences.

Results

Despite the profiles SL01 and SL02 being parallel, 75 km apart, and in the same sedimentary basin, each multi-channel seismic image shows a very different sedimentary stratigraphy and basement geometry (Figure 4). While the southern SL01 MCS record-section shows some chaotic patterns, with heterogeneous layers, sometimes truncations, and a basement with a quite irregular topography, the SL02 MCS record-section, shows some plan-parallel layers (except the seafloor, that is quite irregular in the proximal part). Sometimes, there are some completely seismically transparent areas, which might be associated with erosional boundaries (Figure 4).

SL01

The SL01 line is a 210 km long and NW-SE oriented profile that spans from the continental slope to the distal basin. It is coincident with the ION-GXT 2275 profile and parallel to the associated SL02 profile; both refraction profiles were planned to study the crustal architecture of the SAB (Figure 1).

At sea, a total of 16 OBS (instruments with four components: Hydrophone plus 3-Comp. Seismometer) were deployed, spaced every 13 km, at water depths of 1 560 m to 4 320 m. The 1376 air-gun shots in SL01 were recorded by all instruments. The quality of the recorded signal is very good. This profile crosses two margin parallel profiles designed to image the segmentation (Evain *et al.*, in prep.): the SL06 profile at the SL01OBS02 and the SL05 profile at the SL01OBS03 in the proximal part.

In the OBS data, several near-offset reflected and associated refracted arrivals are visible, decreasing in number as we move towards the distal basin.

From SL01OBS01 onward, the full subsurface sedimentary, crustal, and mantellic sequence is imaged from shots at the vertical of each OBS to offsets reaching 110 km. In addition to clear Pg1, Pg2, Pg3, Pu, Pn (mostly) first arrivals (represented with blue, violet and magenta shades), Ps1 to Ps6 sedimentary refracted arrivals, traveling with apparent velocity increasing from less than 2 km/s (close to the water-cone) up to 3 km/s, are observed as secondary arrivals (represented with red, orange, yellow, and light-green shades). The shallowest layer, is very slow (1.85 km/s) and not very well marked on the seismic profile, but is necessary to fit correctly the secondary later arrivals. From the second to fifth layer, the velocity increases from 2.00 km/s to 3.10 km/s. From SL01OBS01 to SL01OBS03, these layers do not show evidence of clear refracted arrivals and were positioned according to the reflected arrivals. The Ps6 refraction shows top and bottom velocities from 3.35 km/s to 3.45 km/s. Furthermore, at near-critical incidence, high-amplitude reflections are observed, particularly from the tops of the lower crust Pg3P, Unknown unit PuP, and Moho PmP on the seaward-side of OBSs. The Pg1 phase presents the shortest offset span (from ~7.5 to 20 km offset, as we can see in the SL01OBS03 (Figure 5); and the largest curvature indicative of larger velocity gradient. The Pg2 extends from 20 to ~50 km offset and Pg3 from 50 to ~80 km offset and present the lowest apparent velocity gradient.

In the distal oceanic part, from 90 to 220 km model distance, from SL01OBS08 (Figure 6) to SL01OBS15 (Figure 7), the data shows only four sedimentary layers and the related phases, Ps1 to Ps4 remain weak, and almost indistinguishable refracted arrival phases that are recorded as a fan of second arrival phases with slightly increasing velocities and relatively low velocity-gradients that emerges from the water cone. These phases were also modelled according to the reflected arrivals.. In the presumed oceanic basin, the Pg1, Pg2 and Pg3 refracted phases form a relatively continuous event in both amplitude and apparent velocity, without sharp inflections indicative of major velocity changes between layers. The PuP phase spans from 0 to 80 km model distance with apparent velocity close to Pg3 in the necking zone. Pn is observed emerging at ~70 km offset with an apparent velocity increasing from 7.90 to more than 8.10 km/s and large amplitude variations both along offset and OBSs.

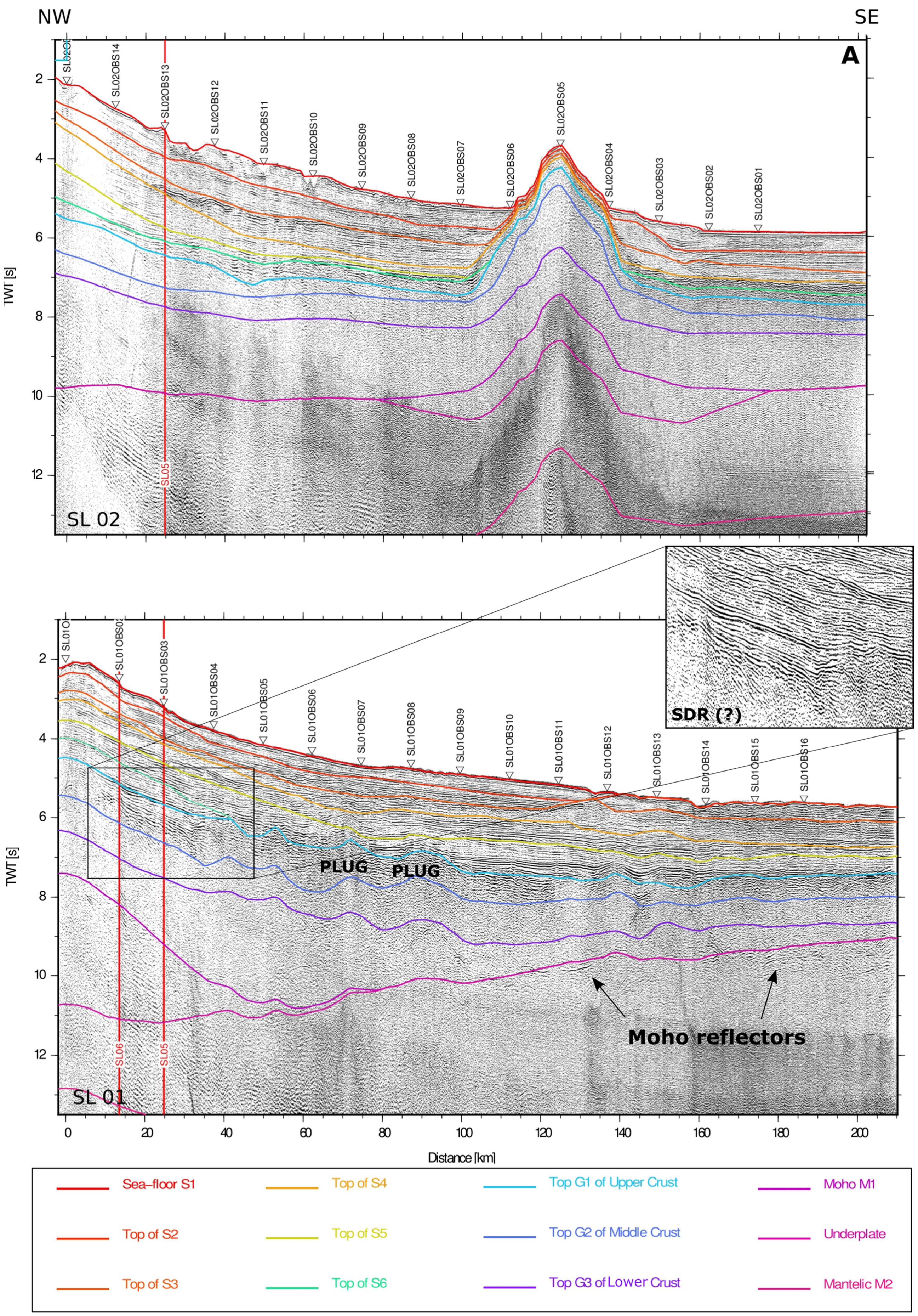
NW
SE
A
SL 02
SL 01
TWT [s]
Distance [km]
SDR (?)
PLUG
PLUG
Moho reflectors
SL05
SL06
Sea–floor S1
Top of S2
Top of S3
Top of S4
Top of S5
Top of S6
Top G1 of Upper Crust
Top G2 of Middle Crust
Top G3 of Lower Crust
Moho M1
Underplate
Mantelic M2

Figure 4: Two-way travel-time record section of MCS data along SL02 (A) and SL01 (B) profiles overlain by time converted interfaces of wide-angle model. The intersections with the SALSA dataset are indicated by red line. OBS locations are indicated by white triangle. Vertical exaggeration at seafloor is 1 :12.5

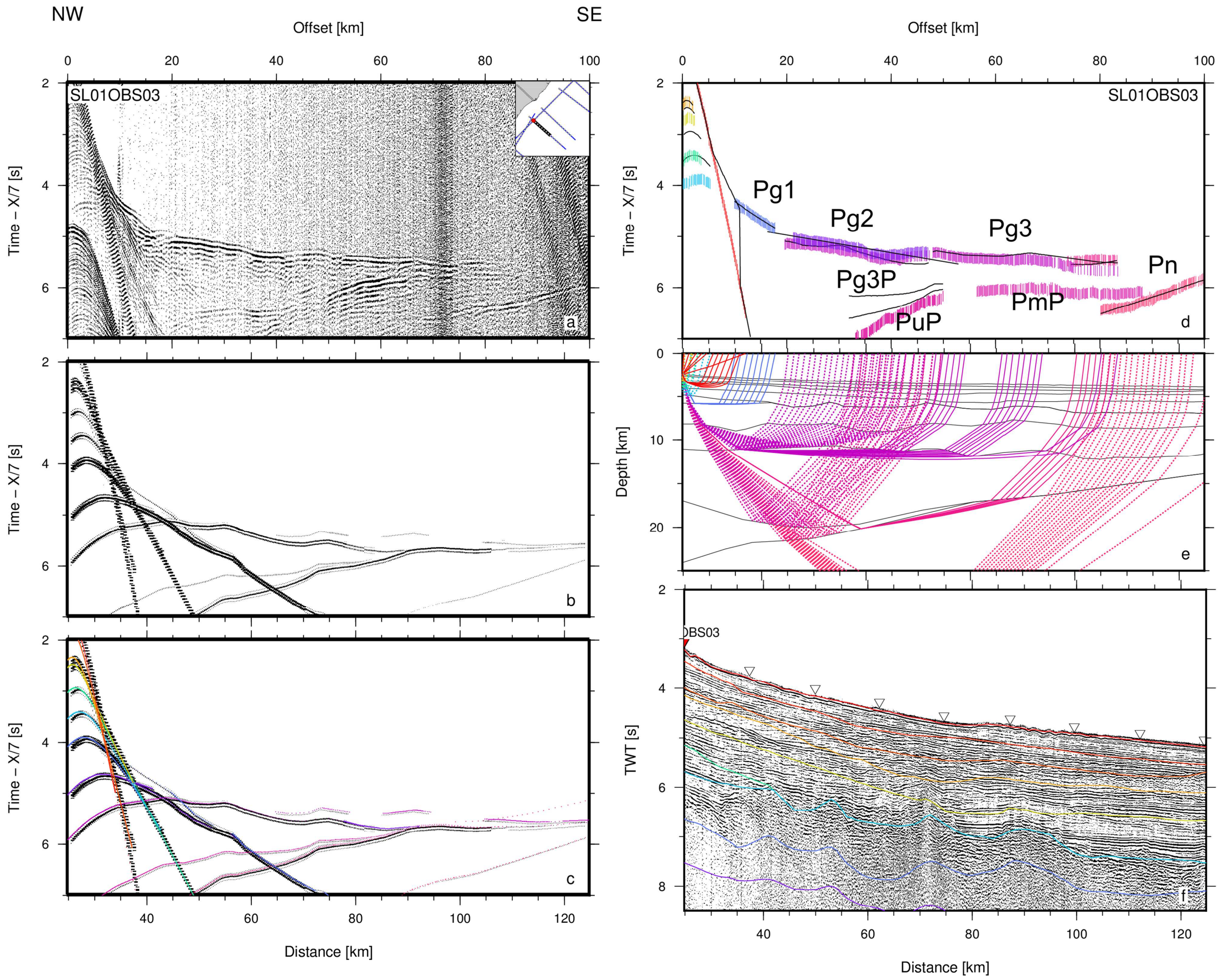

Figure 5: SL01OBS03 on profile SL01 on the SAB. a) Seismic record; b) Synthetics; c) Color coded synthetic; d) Color coded observed travel-times overlain by predicted times in black; e) Seismic rays; f) MCS time migrated section and color-coded model interfaces. On a, b, c, and d, travel-time is reduced by a velocity of 7 km/s.

Velocity model

From SL01 wide-angle data, we digitized 25741 events and interpreted their respective phases. Travel-time uncertainty was estimated on the SL01OBS records and fixed at 0.030 s for the water, 0.050 s for the sedimentary arrivals increasing to 0.100 s for the crustal and mantellic arrivals. The model explains the travel-time and phase of 21204 events or 82% of total picks, with a global RMS travel-time residual of 0.119 s. Given our events individual uncertainty, the model results in a normalized chi-squared of 1.406. Generally, the SL01 model correctly explained the SL01OBS with chi-squared and rms acceptable values (Table 1).

The final velocity model of profile SL01 images all the sedimentary and basement layers to a depth of around 25 km (Figure 8B).

The model has a sedimentary cover with 6 sedimentary layers in the continental part and 4 layers in the presumed oceanic basin, that reach a thickness of 5 km for all along the profile. S1 has no lateral velocity gradient with top and bottom seismic velocities of 1.75 km/s to 1.80 km/s. S2 has a lateral gradient in the velocities that goes from 2.00 km/s in the western part of the profile and gradually decreases up to 1.80 km/s. The two first sedimentary layers pinch out at 130 km in the distal basin.

phase	npts	Trms (s)	chi-squared	Uncertainty (ms)
water	2112	0.028	0.080	30
Ps1P	264	0.091	0.827	50
Ps2P	10	0.076	0.641	50
Ps3P	527	0.087	0.751	50
Ps4P	672	0.186	3.463	50
Ps5P	243	0.097	0.943	50
Ps6P	682	0.252	6.379	50
Pg13	810	0.106	1.122	100
Pg1P3	1582	0.104	1.081	100
Pg23	1507	0.100	1.008	100
Pg33	2173	0.100	1.004	100
Pg3P3	4916	0.127	1.605	100
Pn3	3048	0.113	1.274	100
PmP3	535	0.204	4.163	100
Pu3	419	0.222	4.924	100
Pup4	1483	0.242	5.859	100

Table 1: Reflected or refracted phase name, number of explained events, residual mean-square, and normalized chi-squared value for the SL01 model.

S3 has top and bottom velocities from 2.40 km/s to 2.50 km/s. S4 has regular top and bottom velocities from 2.85 km/s to 3.00 km/s. S5 has also regular top and bottom velocities from 3.10 km/s to 3.15 km/s on the distal basin and a constant velocity of 2.95 km/s on the continental slope. S6 appears only in the continental slope zone, over a basement depression, and pinches out at 40 km and has top and bottom velocities from 3.35 km/s to 3.45 km/s.

The lithospheric structure has five layers: upper crust, middle crust, lower crust, anomalous velocity zone and lithospheric mantle. The upper crust has a thickness of 2.5 km on the continental slope and decreases to 1.0 km and 1.5 km on the distal basin with a very irregular topography, full of basins and mounts, with velocities at the top and bottom of 5.00 km/s and 5.10 km/s, a little decrease to 4.85 km/s at 110 km and increases to 5.10 km/s and 5.20 km/s at the distal basin. The middle crust has regular thickness of 2.5 km for all along the profile, with velocities at the top and bottom from 6.50 km/s to 6.60 km/s. The lower crust starts with a thickness of 5 km in the very northwestern part of the profile, and thickens to 10 km between 20 and 70 km and thins to 3.0 km towards the ocean, with velocities at the top and bottom from 7.00 km/s to 7.20 km/s.

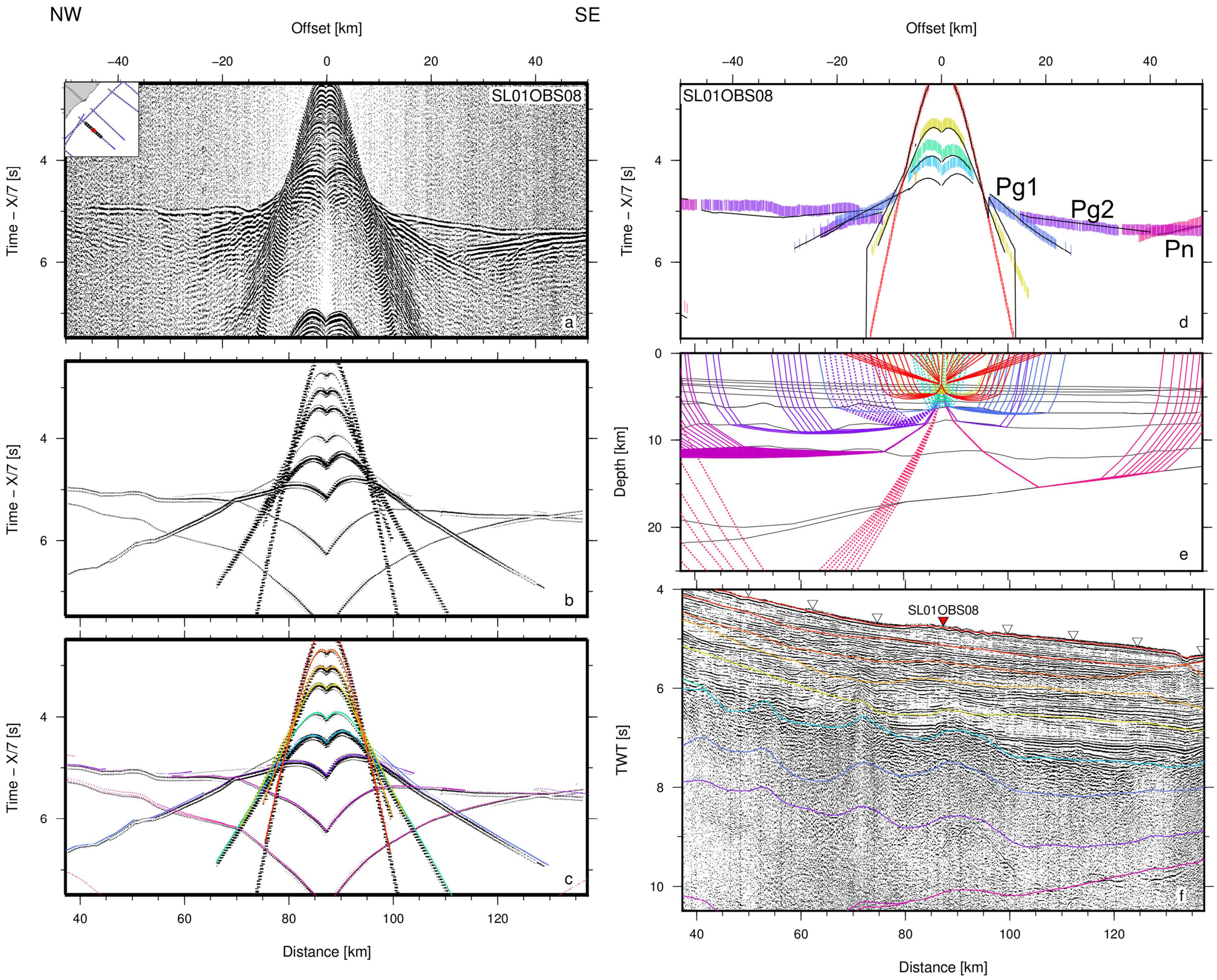

Figure 6: SL01OBS08 on profile SL01 on the SAB. a) Seismic record; b) Synthetics; c) Color coded synthetic; d) Color coded observed travel-times overlain by predicted times in black; e) Seismic rays; f) MCS time migrated section and color-coded model interfaces. On a, b, c, and d, travel-time is reduced by a velocity of 7 km/s.

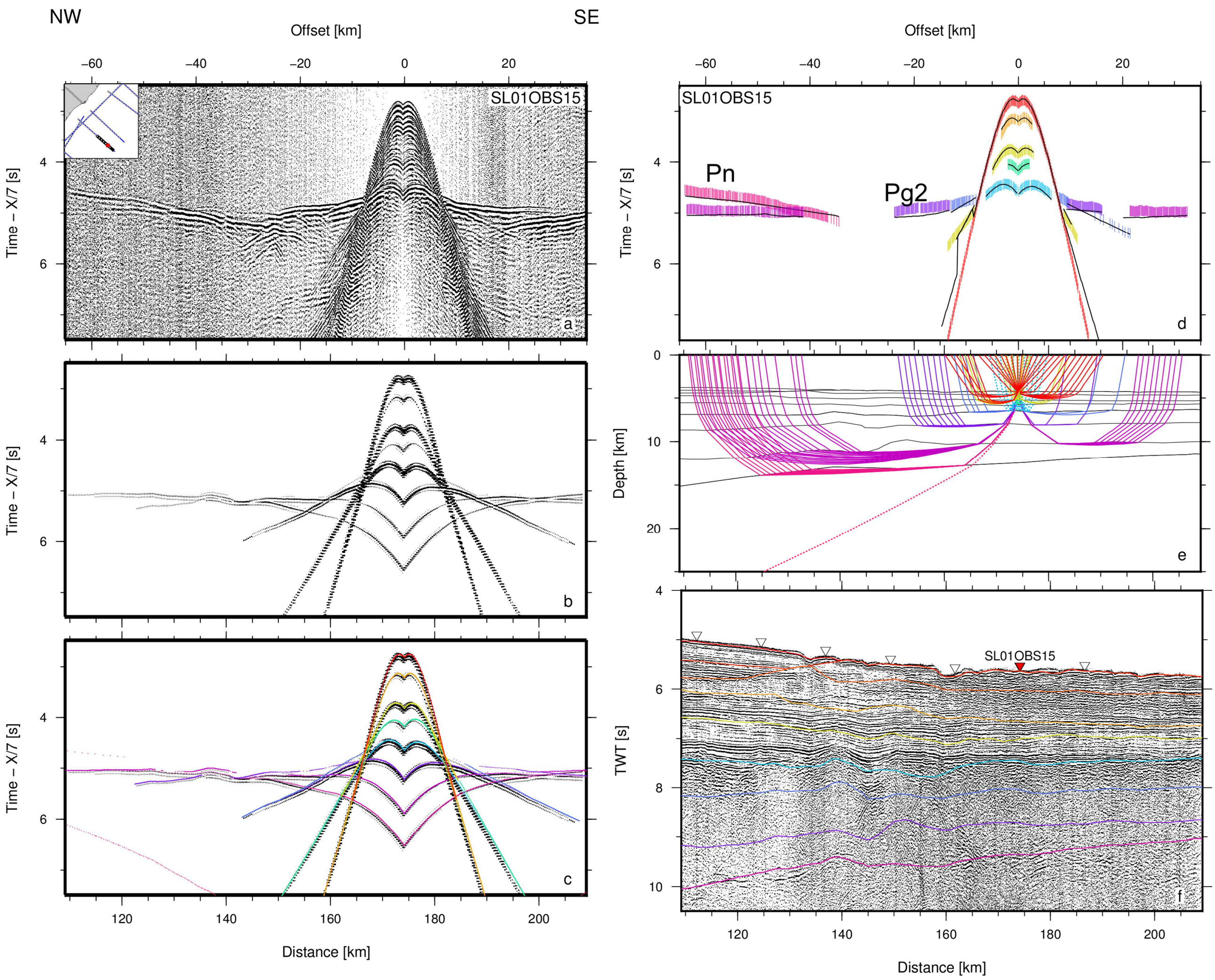

Figure 7: SL01OBS15 on profile SL01 on the SAB. a) Seismic record; b) Synthetics; c) Color coded synthetics; d) Color-coded observed synthetic; d) Color coded observed travel-times overlain by predicted times in black; e) Seismic rays; f) MCS time migrated section and color-coded model interfaces. On a, b, c, and d, travel-time is reduced by a velocity of 7 km/s.

The anomalous velocity zone, located at the necking zone, is badly constrained, showing its possible reflected arrival only in the two most proximal OBSs. These reflected arrivals can also be the result of an internal reflector, representing some intra-crustal body. With this information and the ION-GXT data (Figure 8B), this zone was modeled with 10 km thickness, that thins abruptly until pinching out against the lower crust at 80 km. This zone presents velocities between the top and the bottom from 7.20 km/s to 7.25 km/s. The top of the lithospheric mantle below the Moho has a velocity of 7.90 km/s. Note that an additional lithospheric layer located at 10 to 15 km below the Moho, with 8.10 km/s, is necessary to provide a gradient capable of explaining the Pn arrivals. It is well constrained in the proximal part of the two profiles, but only in the distal part of SL02 profile (Figure 8A).

SL02

The SL02 line is a 220 km long and NW-SE oriented profile, parallel to SL01, that spans offshore from the continental platform to the distal basin. The SL02 was extended inland along a distance of 150 km from the most proximal OBS, for a total profile length of 370 km. It is coincident with the ION-GXT 2300 profile (Figure 8A).

At sea, a total of 15 OBS (instruments with four components: Hydrophone plus 3-Comp. Seismometer) were deployed, spaced every 13 km, at water depths of 1.557 to 4.368 m (Figure 1C). The 1271 air-gun shots in SL02 were recorded by all instruments. The quality of the recorded signal is very good. Inland, the profile was extended 150 km towards the North-West with the deployment of 21 Land Seismic Stations (LSS, spaced every 5 km). The profile has 100 km of extension because, unfortunately, there is a gap of about 50 km between the last LSS and the first OBS, on the inner shelf. This profile crosses the SL05 profile at the position of the SL02OBS02 and SL05OBS14, in proximal position.

The geometry of the sedimentary and crustal layers onland beneath the seismic land stations can further be constrained from geological and geophysical studies conducted in the study area (Chang *et al.,* 1992; Soares *et al.,* 2010; Tavares *et al.,* 2012; de Lima *et al.,* 2015). Surface geology indicates the Sergipano Fold Belt from SL02LSS11 to SL02LSS01, and an outcrop of Quaternary deposits from SL02LSS21 to SL02LSS10, as shown at the SL02LSS15 (Figure 9).

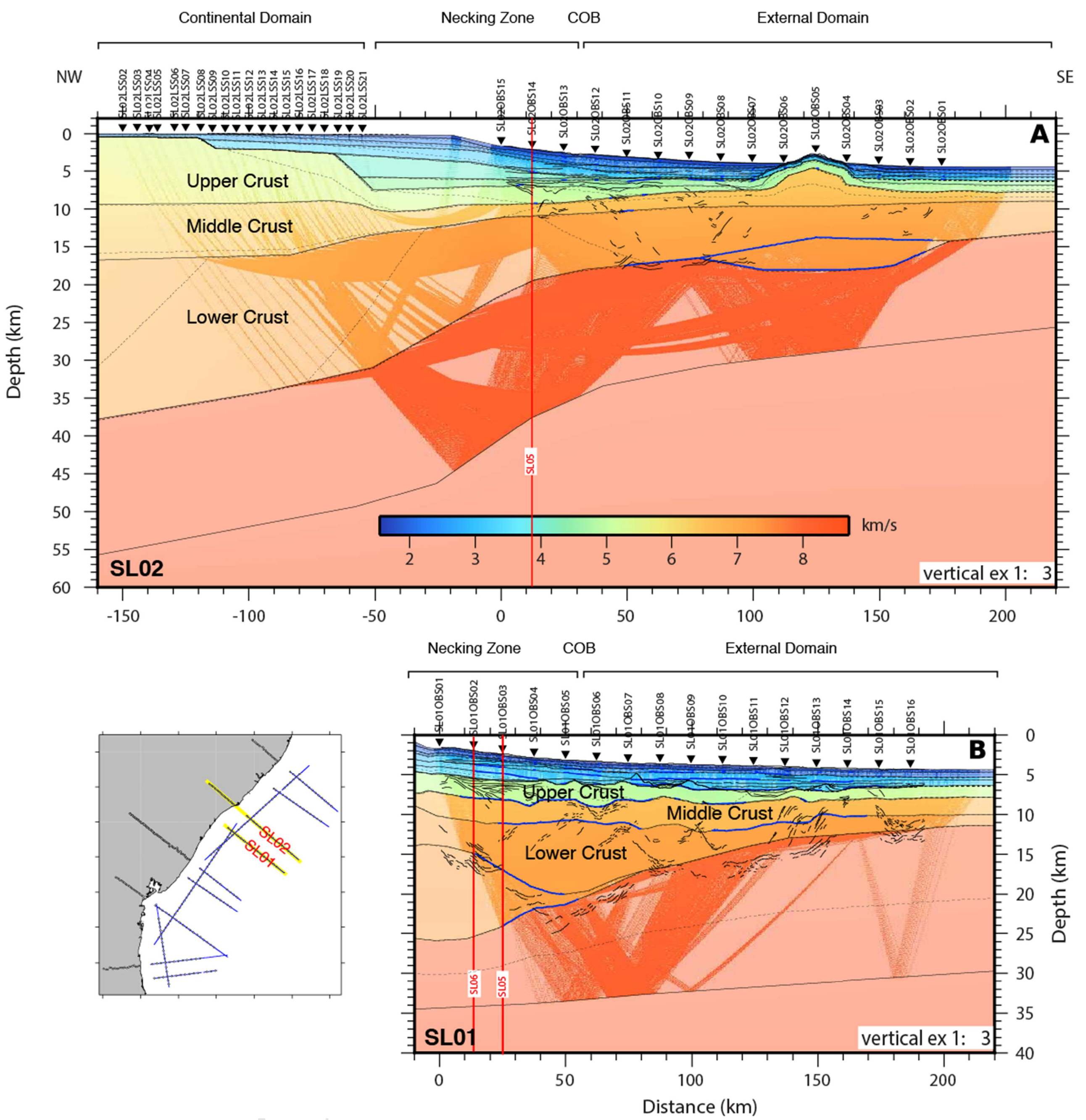

Figure 8: Final P-wave interval velocity models along SL02 (A) and SL01 (B) profiles overlaid by the respective line-drawing of the ION-GXT lines. Black lines mark model layer boundaries. Colored area is constrained by seismic rays. Inverted black triangle mark OBS and LSS positions. Thick blue lines mark the interfaces where reflections are observed on the wide-angle records. Black dotted lines correspond to isocontours. Vertical red lines indicate crossing profiles. Vertical exaggeration is 1:3.

Refracted events in the continental crust middle-crust Pg2 in light-blue, lower-crust Pg3 in blue and Pn in violet are relatively strong and allow to constrain the crustal structure from –160 to 0 km model-distance (Figure 9). Pn arrivals refracted from as deep as 30 km beneath the un-thinned continental margin traveling at 8 km/s apparent velocity. PmP arrivals from 150-160 km offset reflect from the hinge-line where the continental crust begins to thin.

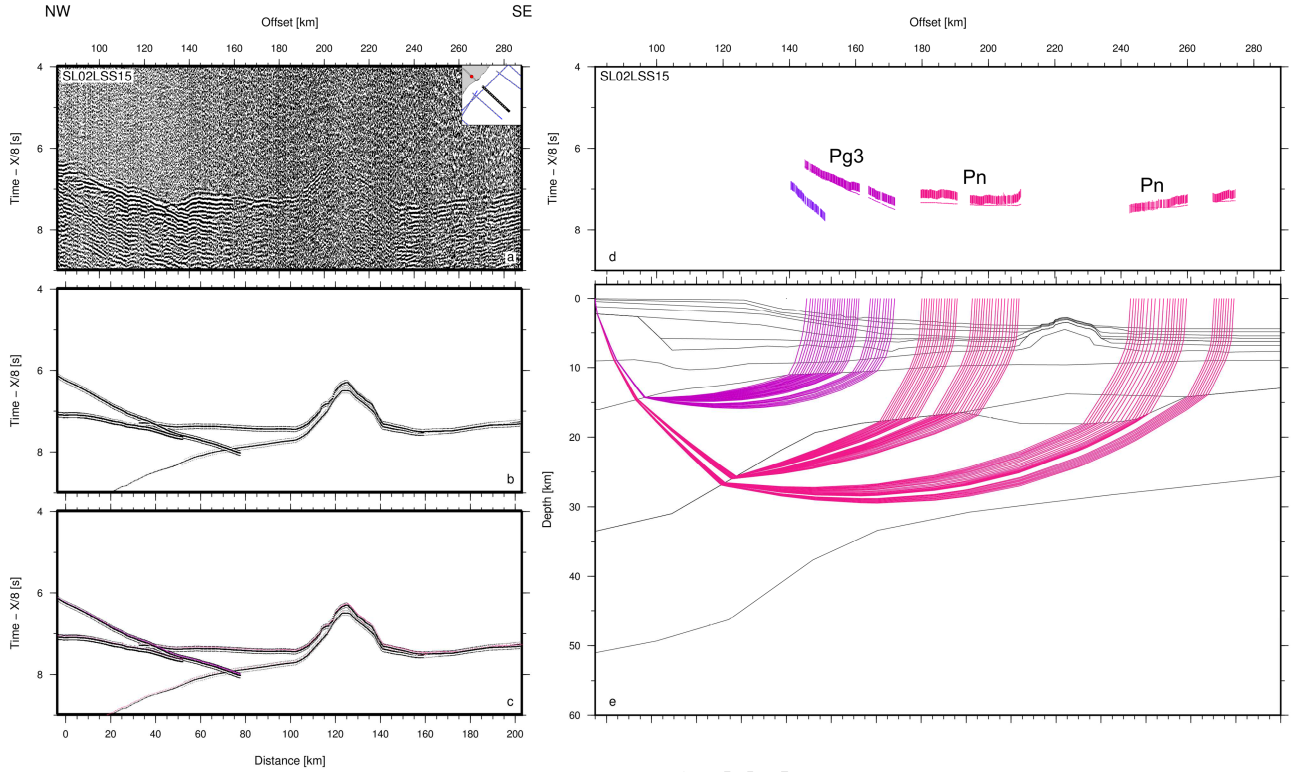

Figure 9: SL02LSS15 on profile SL02 on the SFB/SAB contact. a) Seismic record; b) Synthetics; c) Color coded synthetic; d) Color coded observed travel-times overlain by predicted times in black; e) Seismic rays. On a, b, c, and d, travel-time is reduced by a velocity of 8 km/s.

From SL02OBS15 onward, the full subsurface sedimentary, crustal and mantellic sequence is imaged from shots at the vertical of each OBS to offsets reaching 110 km. The SL020BS14 (Figure 10) shows the example of this part. In addition to clear Pg1, Pg2, Pg3, Pu, Pn (mostly) first arrivals (represented with blue, violet and magenta shades), Ps1 to Ps6 sedimentary refracted arrivals, traveling with apparent velocity increasing from less than 2 km/s (close to the water-cone) up to 4 km/s, are observed as secondary arrivals (represented with red, orange, yellow, and light-green shades). At ~60 km distance, the Ps5 disappears, and the profile continues seawards with only 5 sedimentary layers. Furthermore, at near-critical incidence, high-amplitude reflections are observed, particularly from the tops of the lower crust Pg3P, unknown unit PuP, and Moho PmP on the seaward-side of OBSs. The Pg1 phase presents the shortest offset range (from ~7.5 to 20 km offset), and the largest curvature indicative of large velocity gradient. The Pg2 extends from 20 to ~40 km offset and Pg3 from 45 to ~80 km offset and the lowest apparent velocity gradient.

In the distal part, from 90 to 140 km model distance, as shown in SL02OBS07 (Figure 11), the Ps1 to Ps4 remain weak and almost undistinguishable refracted arrival phases that are recorded as a fan of second arrivals with slightly increasing velocities and relatively low velocity-gradients that emerges from the water cone. The Ps5 refraction shows considerably higher amplitude and apparent velocity: the exact nature of the S6 layer represented by this phase must be further examined from the pre-stack depth migration of the MCS data, for instance. In the distal oceanic part, the Pg1, Pg2 and Pg3 refracted phases form a relatively continuous event in both amplitude and apparent velocity, without sharp inflections indicative of major velocity changes between layers. The Pu phase spans from 90 to 140 km offset and has an apparent velocity close to Pg3. Pn is observed

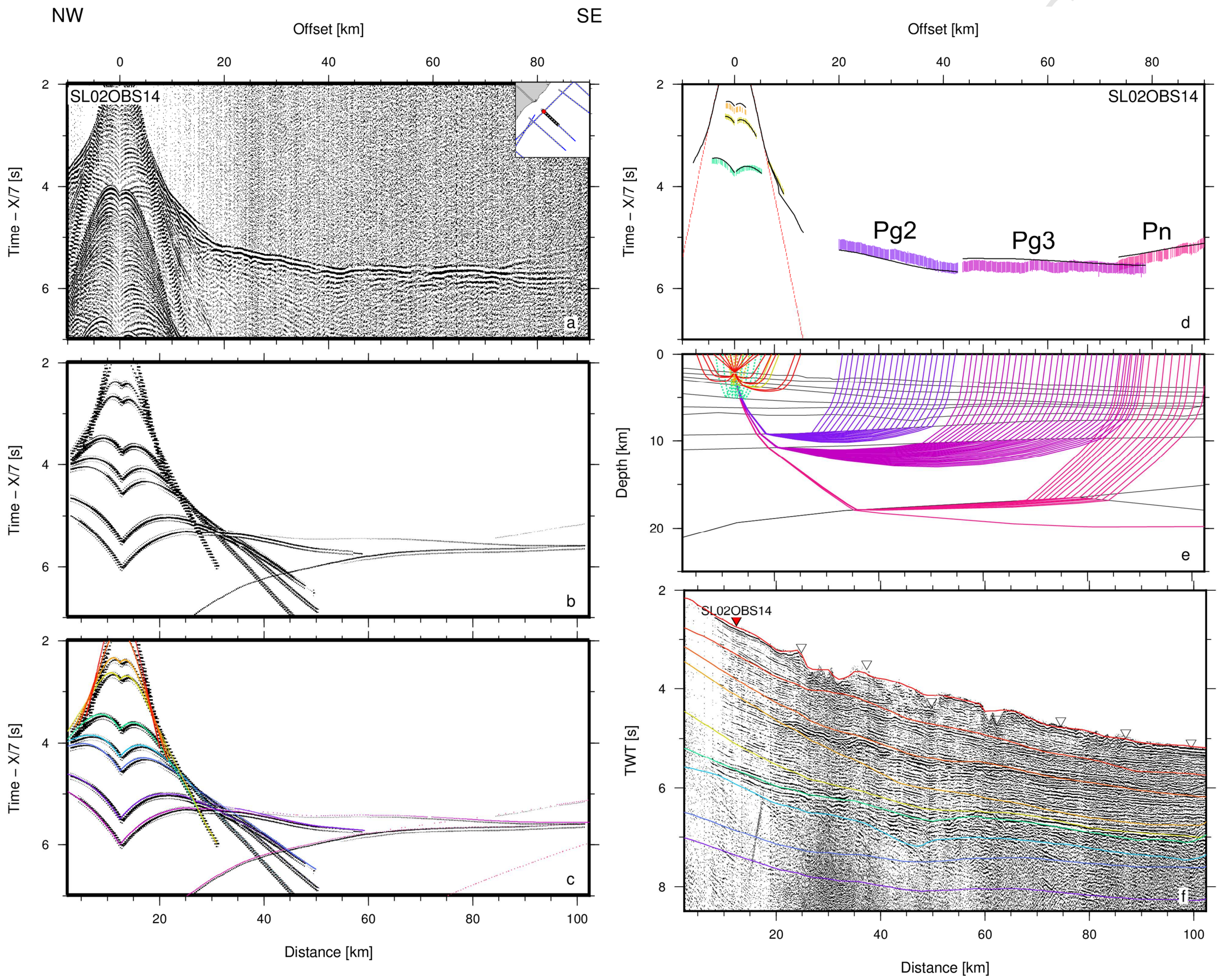

emerging at ~75 km with an apparent velocity increasing from 7.9 to more than 8.15 km/s and large amplitude variations both along offset and OBSs.

Figure 10: SL02OBS14 on profile SL02 on the SAB. a) Seismic record; b) Synthetics; c) Color coded synthetic; d) Color coded observed travel-times overlain by predicted times in black; e) Seismic rays; f) MCS time migrated section and color-coded model interfaces. On a, b, c, and d, travel-time is reduced by a velocity of 7 km/s.

Velocity Model

From SL02 wide-angle data, we digitized 24009 events and interpreted their respective phases. Travel-time uncertainty was estimated on the SL02OBS and SL2LSS records and fixed at 0.030 s for the water, 0.050 s for the sedimentary arrivals increasing to 0.100 s for the crustal and mantellic arrivals. The model explains the travel-time and phase of 21166 events or 88% of total picks, with a global RMS travel-time residual of 0.138 s. Given our events individual uncertainty, the model results in a normalized chi-squared of 1.892. Generally, the SL02 model correctly explained the SL02OBS and SL02LSS with chi-squared and rms values acceptable (Table 2).

phase	npts	Trms	chi-squared	Uncertainty (ms)
water	2708	0.029	0.084	30
Ps1P	21	0.013	0.017	50
Ps2P	436	0.070	0.496	50
Ps3P	305	0.085	0.727	50
Ps4P	298	0.067	0.444	50
Ps5P	122	0.154	2.394	50
Ps6P	277	0.102	1.042	50
Pg1	43	0.113	1.308	100
Pg1P	32	0.186	3.570	100
Pg2	347	0.167	2.793	100
Pg2P	30	0.052	0.282	100
Pg3	1893	0.131	1.706	100
Pg3P	1980	0.121	1.470	100
Pn	7194	0.121	1.462	100
PmP	1083	0.145	2.101	100
Pu	38	0.052	0.274	100
PuP	1078	0.243	5.906	100

Table 2: Reflected or refracted phase name, number of explained events, residual mean-square, and normalized chi-squared value.

The final velocity model of profile SL02 images the depth geometry of all sedimentary, crustal and mantellic layers to a depth of around 34 km (Figure 8A). According to the interpretation of the wide-angle data described above the velocity structure of SL02 model was modeled using four to six layers of sediments. These sedimentary layers are characterized by relatively homogeneous P-wave velocities all along the SL02 model with no strong lateral variation. This sedimentary deposit in the SAB starts at –120 km model distance and reaches a maximum of 7 km of thickness between -50 and -20 km model distance until 2.5 km at the SE in the distal basin (Figure 8A).

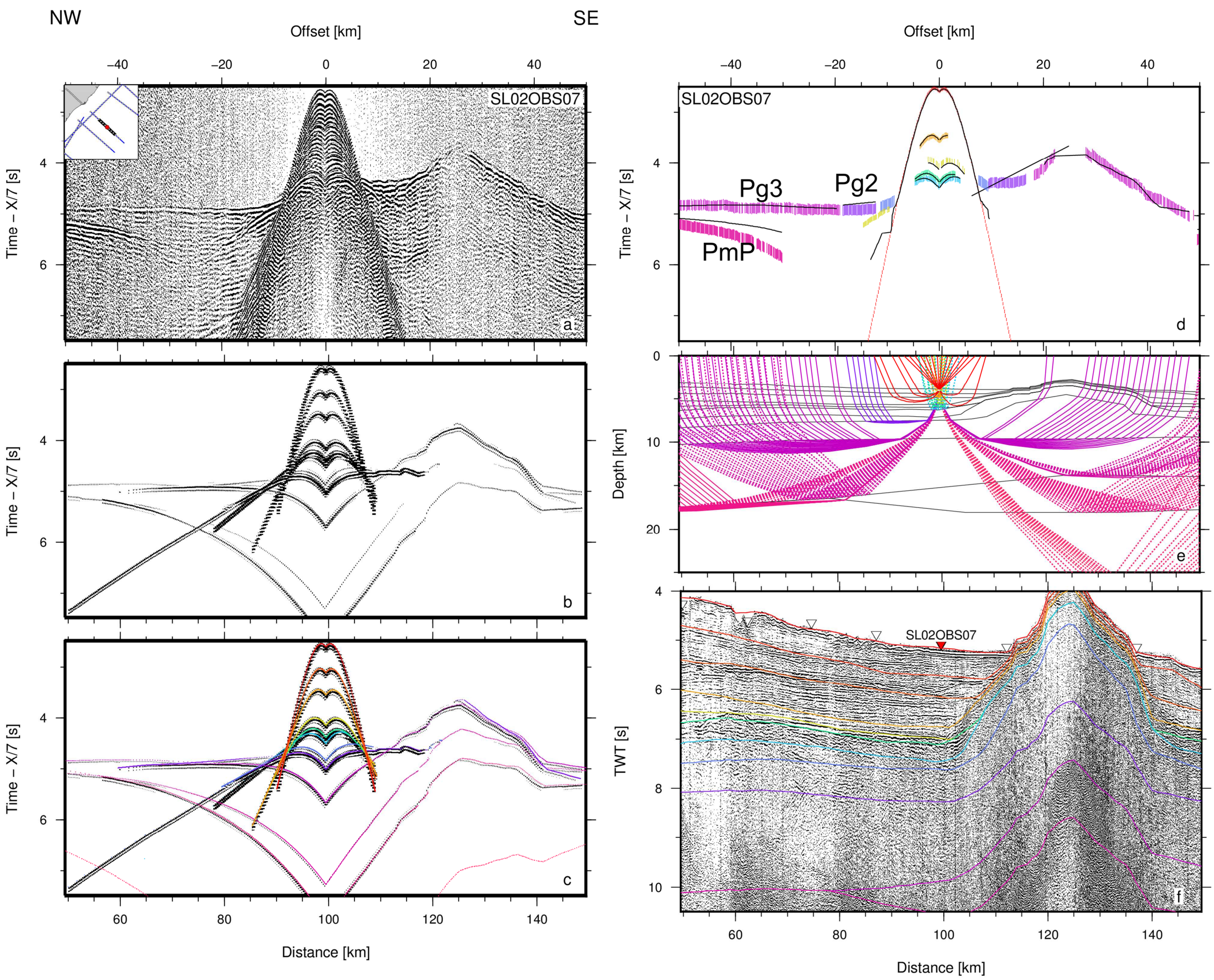

Figure 11: SL02OBS07 on profile SL02 on the SAB. a) Seismic record; b) Synthetic; c) Color coded synthetic; d) Color coded observed travel-times overlain by predicted times in black; e) Seismic rays; f) MCS time migrated section and color-coded model interfaces. On a, b, c, and d, travel-time is reduced by a velocity of 7 km/s.

The P-wave velocities of the sedimentary sequence show an increasing trend: the top velocity at the seafloor is 1.65 km/s (S1) and the maximum velocity 4.7 km/s is reached at the base of the sedimentary sequence (S6).

S1 has top and bottom P wave seismic propagation velocities of 1.65 km/s to 1.85 km/s. S2 has a negligible vertical gradient and propagation velocity of 2.2 km/s on the western end of the profile that gradually decreases up to 2.10 km/s. S3 has top and bottom velocities from 2.60 km/s to 2.70 km/s with a small gradient decrease towards the continental slope. S4 has top and bottom velocities from 3.00 km/s to 3.25 km/s. S5 has top and bottom velocities from 4.10 km/s to 4.20 km/s. S6 has constant top and bottom velocities from 4.60 km/s to 4.70 km/s.

Beneath this sedimentary record, the top of the basement corresponds to a rough interface and the modeled basement structure comprises four crustal layers: upper crust, middle crust, lower crust and an anomalous body under the volcano. The upper crust has a thickness between 1.0 km and 2.0 km on the presumed oceanic basin and increases to 3.0 km at the continental slope, with velocities at the top and bottom from 4.75 km/s to 5.1 km/s.

The middle crust has a regular thickness of 3.0 km for all the profile, except under the volcano, where it reaches almost 5.0 km with velocities at the top and bottom from 6.4 km/s to 6.5 km/s on the continental slope and from 6.2 km/s to 6.3 km/s on the distal basin. The lower crust is 8.0 km thick at the northwestern end of the model and completely thins out to 4.0 km thick towards the ocean, with velocities at the top and bottom from 6.90 to 7.10 km/s along all the profile, except in the necking zone, between 0 and 50 km model distance, where there is a slight increase of the velocities in the middle and the lower crusts: the middle crust passes from 6.10-6.30 km/s to 6.30-6.50 km/s and the lower crust, from 6.90-7.10 km/s to 7.30-7.50 km/s (Figure 8B). Note that there is also a thick anomalous body, not located below the Necking Zone as along SL01 profile, but below the Moho in the volcanic edifice area. It has a thickness of 8 km and velocities between 7.3-7.4 km/s.

Evaluation of the models

Gravity modelling

A 2-D model consisting of homogeneous density blocks was constructed from the seismic velocity model: the P-wave velocity is converted to densities according to Ludwig *et al*. (1970) except onshore in the continental crust where conversion follows Christensen and Mooney (1995). The resulting density ranges from 2200 to 2500 kg/m³ in the basin, 2600 to 2750 kg/m³ in the crust and 3000 to 3170 kg/m³ in the under-crustal unit. The mantle density is set at 3420 kg/m³. The model is extended down to 80 km where isostatic compensation may be reached, and the modeled free-air anomaly is compared to measured gravity anomaly along the SL01 and SL02 profiles (Figure 12).

The SL01 model fits relatively well (within less than 10 mGal) the gravity data acquired offshore during the SALSA survey, except for the continental slope (where the model is less constrained) where there's a misfit of 17 mGal. Free air gravity from satellite data (Sandwell *et al.*, 2014) extracted along the profile and 10, 20, and 30 km cross-line presents broad (>50 km wavelength) along profile and lateral scatter amplitude variations of +/- 10 mGal (Figure 12c and d).

The SL02 model fits relatively well (within less than 25 mGal) the gravity data acquired offshore during the SALSA survey, except for the seamount where there's a misfit of 65 mGal, probably due to the 3D effects. The calculated gravity anomaly falls well within the values observed on parallel profiles extracted north and south of the profile (Figure 12a and b), derived from satellite gravity measurements (Sandwell *et al.*, 2014). Due to the high altitude of the satellite, lower wave-length are not well recorded.

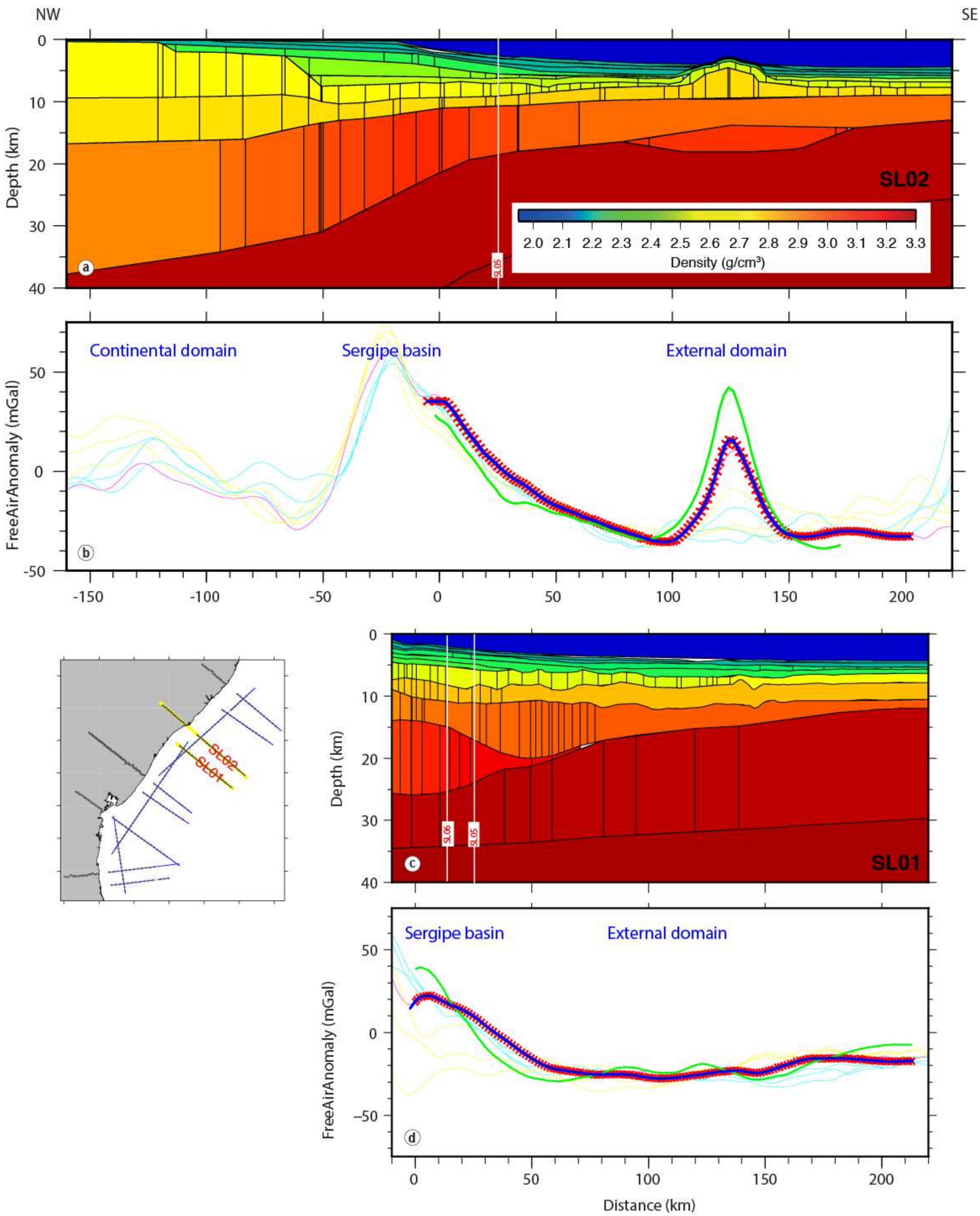

Figure 12: *Gravity modeling along SL02 profile. a) Density model up to a depth of 40 km overlain by interfaces from wide-angle modeling. b) Free-air gravity anomaly observed (Pavlis et al., 2012 for the offshore data and BGI: International Gravimetric Bureau, for the land data) along the SL02 profile (red crosses) and laterally 10, 20 and 30 km (SW-ward as yellow lines, NE-ward as cyan lines), measured during the SALSA experiment (blue line) and calculated (green line). Gravity modeling along SL01 profile. c) Density model up to a depth of 40 km overlain by interfaces from wide-angle modeling. d) Free-air gravity anomaly observed (Pavlis et al., 2012) along the SL01 profile (red crosses) and laterally 10, 20 and 30 km (SW-ward as yellow lines, NE-ward as cyan lines), measured during the SALSA experiment (blue line) and calculated (green line).*

Hitcount, spread, and resolution

Interface depth node spacing as well as velocity node spacing is key to model the lateral variations of the seismic velocity with sufficient resolution, but without introducing spurious and unwarranted complexity. Although all synthetics section correctly reproduces the observed amplitude on the wide-angle data (Figures 5 to 11), suggesting a good parameterization of the model, we perform evaluation tests of the P-wave velocity models: hitcount, Spread Point Function (SPF) and resolution (Figure 13).

The interface nodes are spaced at less than 2 km on the seafloor where depth is well constrained by multi-beam bathymetry. Node spacing increases to 2.5 km for the three first sedimentary layers then 5 km for the deepest sedimentary layers and the basement where the interface geometry is well constrained in twt from the MCS data, then 10 km for the middle crust, 15 km for the lower crust and Moho, 30 km and 50 km for the intra-mantellic reflectors. The velocity nodes are not spaced evenly but located where velocity changes are warrant by the observed wide-angle records, resulting in node spacing ranging from 30 to 350 km. The total standard deviation for depth nodes and velocity nodes is 6.229 km and 1.785 km/s, respectively. Most interface and velocity nodes in our experiment produce a hit-count larger than 3000 rays (Figure 13) with exception of the edges of our survey and the middle crust. The Spread Point Function (Figure 13) is indicative for a given velocity variation of the resulting travel-time variations when taking the different ray paths into account. Depth and velocity node SPF is relatively homogeneous in the models except in the lower crust along SL02 profile in the transition of the continental to the presumed oceanic domain. Finally, the diagonal terms of the resolution matrix are a measurement of the spatial averaging of the true earth structure by a linear combination of model parameters (Zelt 1999). Typically, resolution matrix diagonals greater than 0.5–0.7 are said to indicate reasonably well-resolved model parameters (e.g. Lutter and Nowack 1990). The major part of the interface and velocity nodes present good resolution (>0.7). Resolution is poorest at the transition zone, in the lower crust, in the upper crust at the SAB, and under the volcanic edifice (Figure 13).

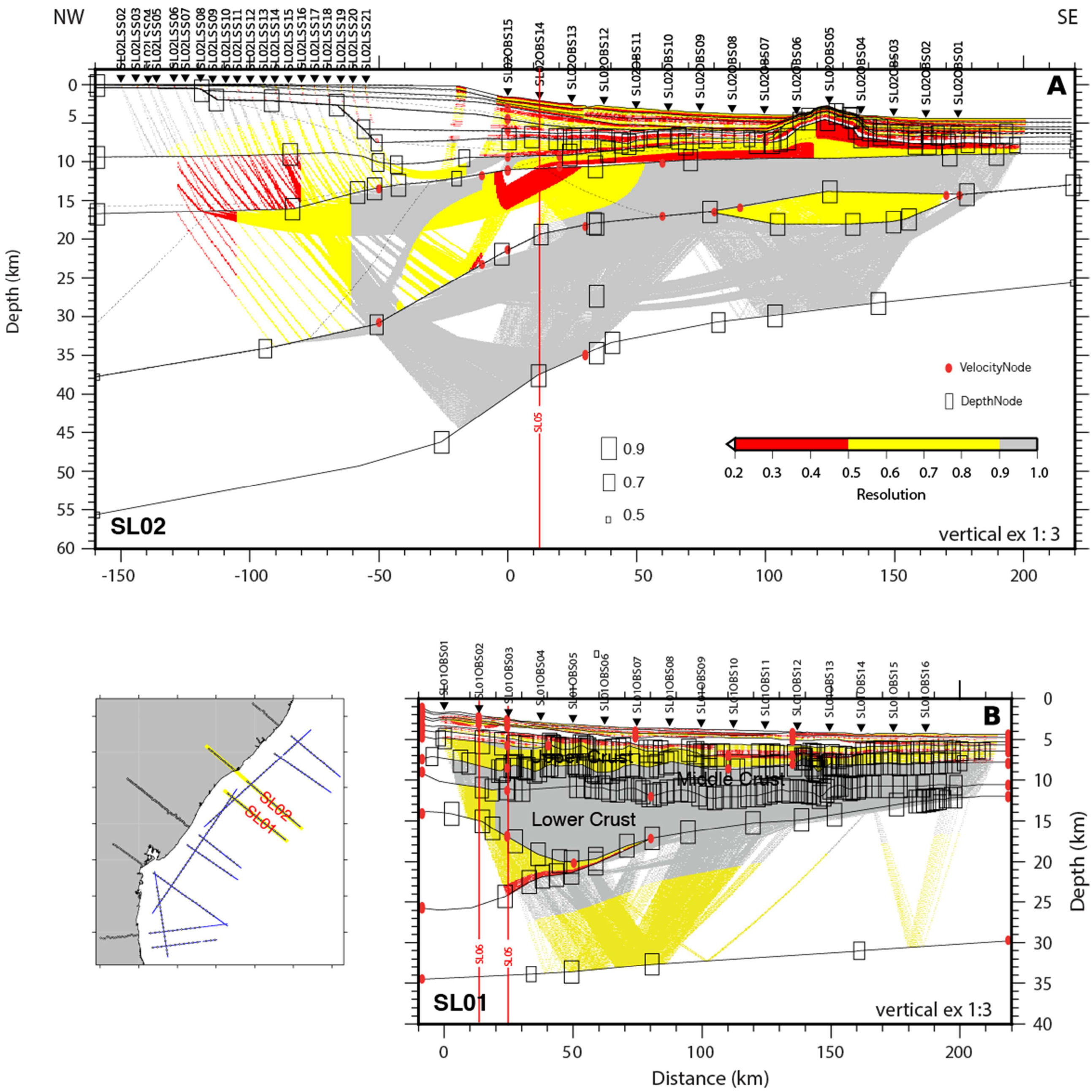

Figure 13: Evaluation of the wide-angle models SL01 (A) and SL02 (B): Resolution of velocity (gridded and colored). There are zones that were not imaged due to the lack of ray coverage.

MCS data pre-stack depth migration (PSDM)

To verify the accuracy of the wide-angle velocity model, the MCS data is pre-stack depth migrated and residual move-out analysis is performed. The pre-processing sequence is identical to the MCS data time processing, and includes geometry, wave-equation multiple attenuation, shot-gather predictive deconvolution, time variant band-pass filter, and random multiple attenuation. The PSDM processing is undertaken using the Seismic Unix package (Stockwell Jr., 1999; Cohen and Stockwell Jr., 2010). The PSDM consists in 2 steps: ray tracing and seismic data depth migration.

First, the velocity model is utilized to compute travel-time tables regularly spaced at 150 m along the profile by paraxial ray tracing on a 50 × 25 m spaced grid, then travel-times in shadow zones are compensated by solving the eikonal equation. Secondly, common offset Kirchhoff depth migration is performed: Migrated traces are output as common image gathers (CIG) binned at 25 m with 30 offset-classes between 249 and 4596 m at 150 m spacing. Dip-independent velocity analysis can then be performed on the migrated CIG by analyzing residual move-out. Hence, if the velocity model used for migration is close to the true medium velocity, all common offset migrated panels map the recorded seismic events to the same reflector depth, else the move-out from near to far offset translates into an interval velocity correction (Liu and Bleistein, 1995). Figure 14 presents the PSDM section and CIG gathers extracted every 7.5 km along the two profiles. Moreover, depth migrated gathers are excellent records of amplitude variations with offset (AVO), and therefore are indicators of in-situ rheological changes. The residual move-out behavior together with the seismic character from PSDM images are key elements to locate accurately major geological contacts, moreover with higher horizontal resolution when compared to the OBS records.

SALSA01 (Fig. 14C) and SALSA02 (Fig. 14A) were migrated up to a depth of 18 km, showing very good resolution in the sedimentary layers, and a good resolution in the crust, with good agreement between strong reflectors and their wide-angle estimated depths. The SAB shows a sedimentary structuration that can be subdivided between upper and lower packages. Upper sediments represent the first 4 layers, which are finely stratified and made of low amplitude continuous reflectors while deeper reflectors have a stronger amplitude character. The entire sedimentary package is clearly interrupted by the volcanic edifice. The upper package varies in thickness from about 1.5 km at the continental slope, 3 km at NW side of the volcano and 2 km at SE side, at the presumed oceanic basin. The lowest sedimentary package is composed by 2 layers that merge into 1 layer, at 40 km model distance on SL01, and at the NW side of the volcano at SL02. The top of this package shows the strongest and most continuous reflector in the MCS data. This reflector represents the base of the Calumbi Formation. A recede at the sea level in the end of the Coniacian controlled the erosion of the underlying sequences. This regional erosional event is represented by the so called Pre-Calumbi Formation (probably Santonian, ~86 Ma) unconformity at the base of the Piaçabuçu Group (Mohriak *et al*., 1998; Campos Neto *et al*., 2007). This unconformity can be observed as the most remarkable reflector, and is interpreted as a regional angular, intra-Cretaceous unconformity in the platform that is almost flat-lying in the deep-water region and overlies horizontal sedimentary layers (Mohriak *et al*., 1998, 2000).

The basement is composed by chaotic seismic facies in the MCS data. Below the basement it is impossible to differentiate any seismic facies or structure. Unlike the profile SL01 (Figure 4), no reflector corresponding to the Moho is observed in the profile SL02.

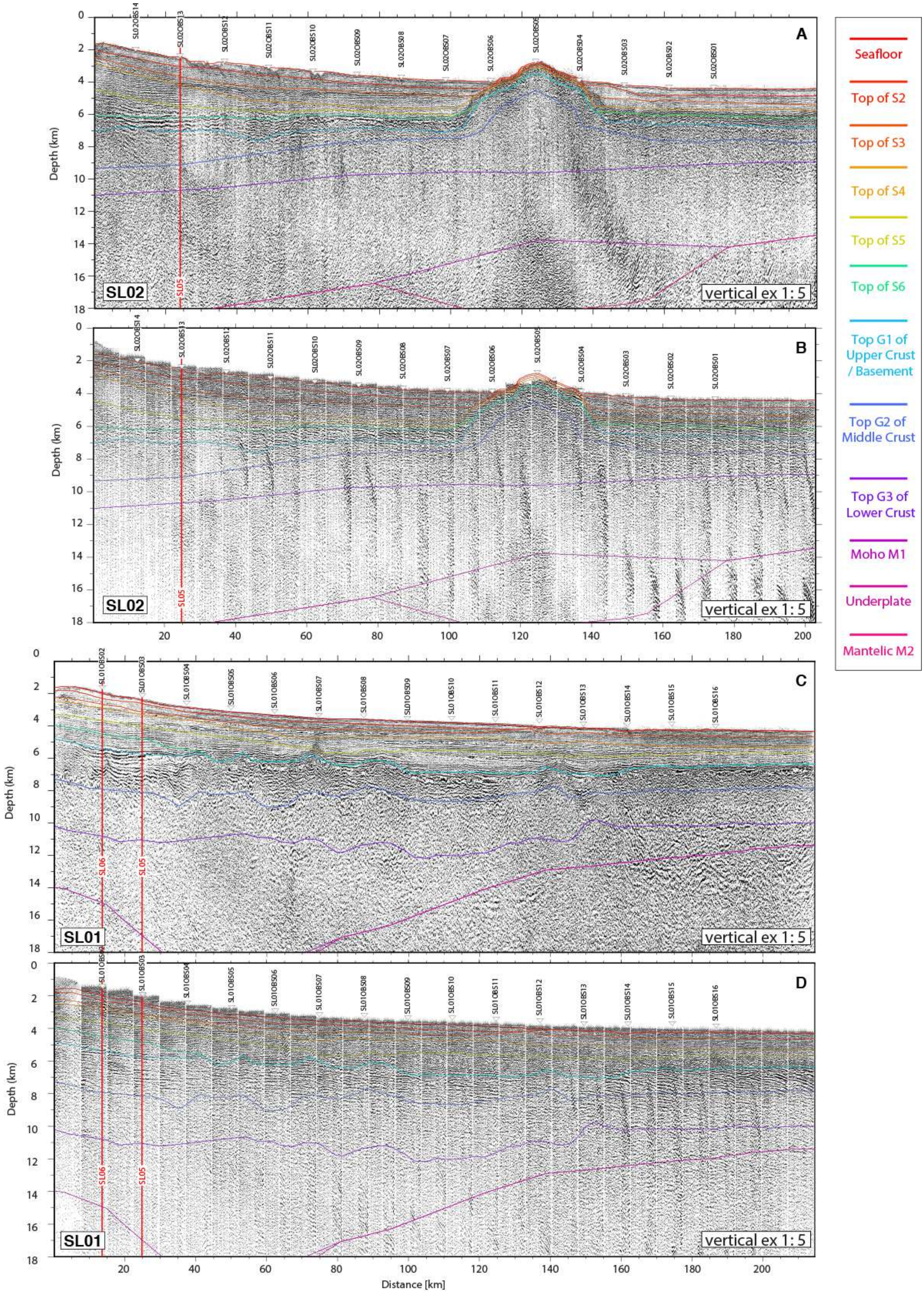

Figure 14: a) Pre-stack depth migrated record section of MCS data along SL02 profile. Model's interfaces are represented with continuous lines. The intersections with the SALSA dataset are indicated by red line. Vertical

exaggeration is 1:5. b) Residual move-out of MCS data along SL02 profile. Common image gathers are spaced every 7.5 km. c) Pre-stack depth migrated record section of MCS data along SL01 profile. Vertical exaggeration is 1:5. b) Residual move-out of MCS data along SL01 profile. Common image gathers are spaced every 7.5 km. Vertical exaggeration is 1:5.

Discussion

In order to constrain the nature of the crust, 1D crustal velocity- depth (Vz) profiles were extracted underneath the top of the basement at a 10 km interval from the final velocity models (Figure 15). These Vz graphs can be compared to compilations for typical continental crust (Christensen and Mooney, 1995) and Atlantic-type oceanic crust (White *et al.*, 1992) that allow to discuss the properties of crust and to establish the lateral segmentation along the profiles.

On the base of this analysis of the final models and these Vz graphs, three distinct domains can be distinguished: 1. Unthinned Continental Domain; 2. a domain of crustal thinning, the Necking Domain; and lastly, 3. an external distal domain interpreted to be of oceanic nature (Figure 15). No transitional domain is defined in the SAB, the transition between the thinned continental and oceanic crusts is direct.

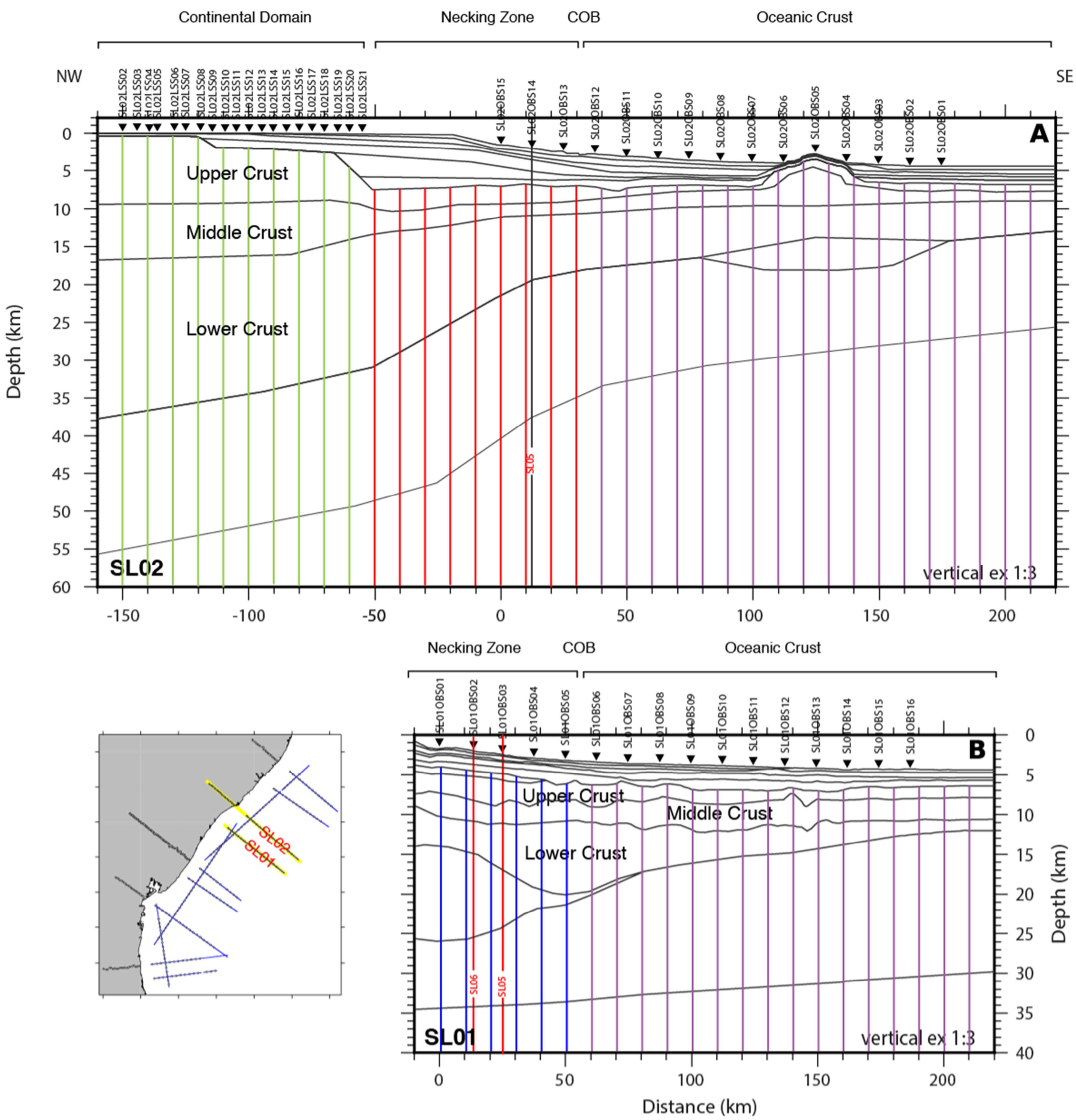

.

Figure 15: Distribution of 1-D velocity profiles extracted from the final P-wave interval velocity model and color coded according to segmentation along the SL02 (A) and SL01 (B) profiles

Unthinned Continental Domain

This domain is essentially based on the profile SL02 data, taking into consideration that it is the unique profile with landstations.

As the inland proximal part of the profile, between the landstations and the OBSs, is not completely constrained by the seismic rays, the modeling of the Unthinned Continental domain, was also constrained by additional information obtained from the crossing with profile SL05 (Evain, *et al.*, In prep.), and bibliographical information (Chang *et al.*, 1992 ; Feijó *et al.*, 1994 ; Mohriak *et al.*, 1995, 1998, 2000; Blaich *et al.*, 2008 ; Soares *et al.*, 2010 ; Tavares *et al.*, 2012 ; de Lima *et al.*, 2015) .

In the Continental domain, the Moho is 27 to 37 km depth below basement (Figure 16). The comparison of the 1D velocity profiles with a worldwide compilation of the continental crust (Christensen and Mooney, 1995) clearly shows similarities both in velocities and gradients with our results (Figure 16).

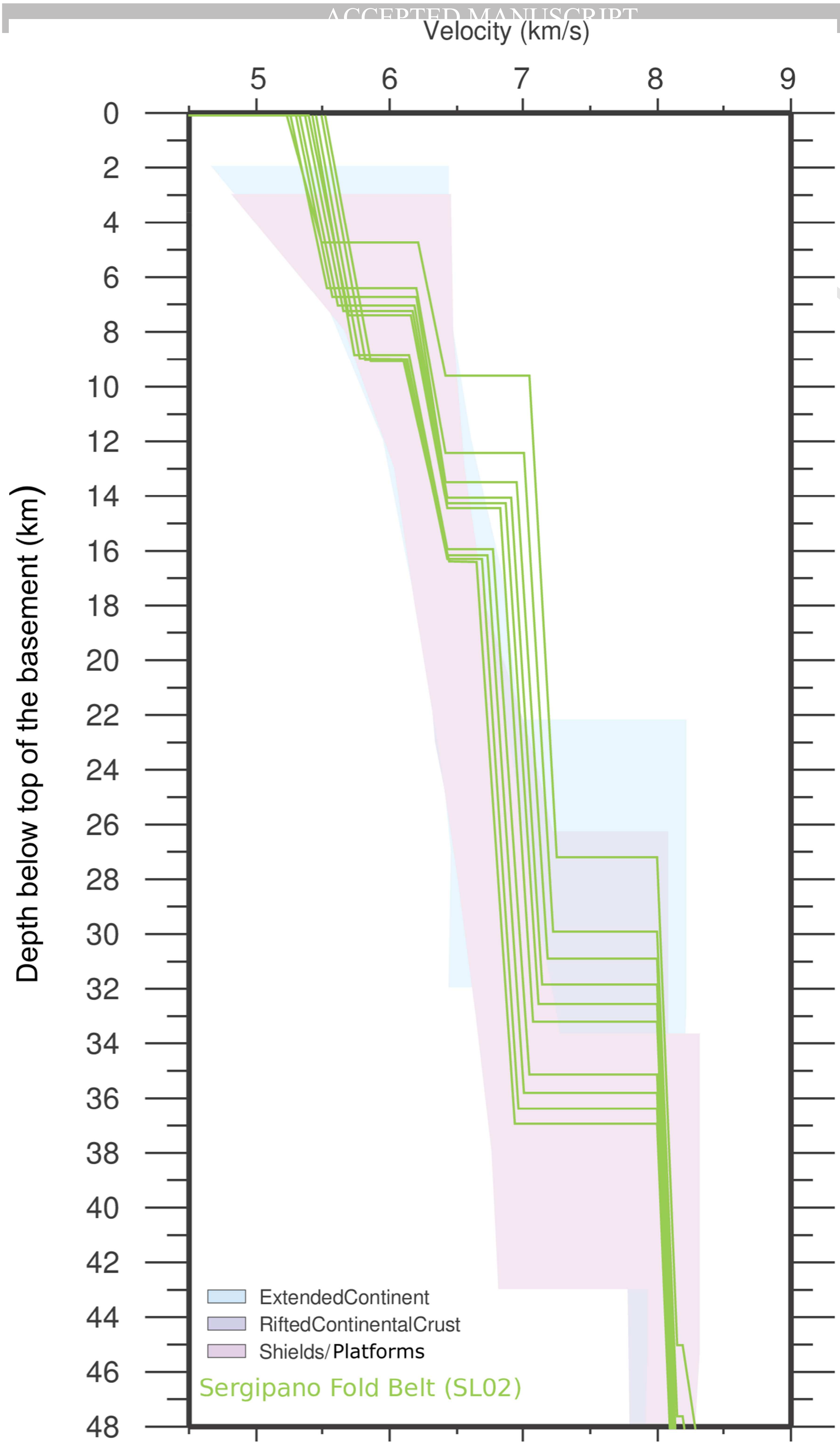

Velocity (km/s)
5
6
7
8
9
Depth below top of the basement (km)
0
2
4
6
8
10
12
14
16
18
20
22
24
26
28
30
32
34
36
38
40
42
44
46
48
ExtendedContinent
RiftedContinentalCrust
Shields/Platforms
Sergipano Fold Belt (SL02)

577

Figure 16: Compilation of 1D velocity-depth profiles extracted below the top of the basement (Vz) in the domains of unthinned continental crust. The light blue areas correspond to averaged velocity profiles for continental crust (Christensen and Mooney, 1995).

At the SL02 profile, in the Continental domain, the top of the upper crust, the basement, is at the surface until -120 km distance model, then it deepens, forming three "stairs", first at -120 km distance model, where it deepens to 2.5 km deep, and then at -60 km distance model it deepens to 8 km deep (Figures 15 and 16). The upper layer has velocities between 5.50 and 5.90 km/s, that decreases seawards. The topography of the interface between the upper and middle crust is almost regular for all along the profile, and the velocities of the middle crust range from 6.10 to 6.50 km/s. The base of the lower crust corresponds to the Moho, whose depth decreases smoothly from 37 to 33 km. Its velocities at the top increase from 6.60 km/s in most continental part, to 7.30 km/s seawards, near to the Necking Zone and its velocities at the base, range from 6.90 km/s at the continental domain to 7.50 km/s near the Necking Zone.

The deep seismic refraction experiment carried out in the Pernambuco Province, northwards (Figure 1) (Soares *et al*., 2010; Tavares *et al*., 2012; Lima *et al*., 2015) shows a structure of the lithosphere, with 2 layers separated at about 16 km depth, with a velocity of 5.75 to 6 km/s at the top and 6.2 to 6.3 km/s at the base of the upper crust, and 6.4 to 6.5 km/s at the top and 6.75 to 6.90 km/s at the base of the lower crust, for a total continental crust thickness of about 32 km. In terms of velocities, this structure is quite similar to that found in SL01 and SL02. The upper layer found by these authors, would correspond to the upper and middle layer of SL01 and SL02.

These similarities put into question the proposition that the SFB is a Neoproterozoic fold–thrust belt produced by inversion of a passive margin basin located at the northeastern edge of the ancient Sao Francisco plate (Almeida *et al*., 1977 ; D'el-Rey Silva, 1999) and constituted by a 42 km thick crust (Oliveira *et al*., 2008) and reinforces the idea that the SFB was possibly on the margin of the Palaeoproterozoic Pernambuco-Alagoas Block (Oliveira *et al.,* 2010), and was attached to the Sao Francisco Craton during the Brasiliano (~600 Ma) orogenic event (Davison and Santos, 1989; Silva Filho, 1998). These results put the limit clearly between the Sao Francisco Craton and the Palaeoproterozoic Pernambuco-Alagoas Block on the Vaza Barris transfer zone, considering it as a major structural fault.

Necking Zone:

The necking zone goes from -55 km to 25 km profile distance. On profile SL02, throughout the necking zone, the total crustal thickness, without the water column (~4 km through the COB) and sediment cover, thins from ~23 km to ~10 km. The thickness of the upper crust thins from 10 km in the limit with the continental domain to only 1 to 2 km seaward in the limit with the oceanic domain. At the depocenter of the SAB, at -50 km distance of the profile, the top of the upper crustal layer deepens to ~8 km and remains at this depth for all along the profile. The thickness of the middle crust thins from ~7 km in the limit with the continental domain, to ~2 km through the necking domain until the COB. The Moho rises from 31 km depth in the limit with the continental domain to ~18 km depth in the COB over a distance of almost 100 km (Figure 8), and the total thickness of the lower crust thins from 19 km in limit with the continental domain to 8 km beneath the COB, with a light velocity increase in the middle of the Necking Zone. The lateral velocity change happens only in the lower crust where it changes from 7.0 to 7.3 km/s on the top and from 7.25 to 7.5 km/s at the base. In the Necking Zone between 30 and 90 km distance, and 9 and 15 km depth, there are also packages of intra-crustal reflectors that may correspond to SDRs. Although the base of the crust is much clearer in SL02 than in SL01, without basal intra-crustal reflectors.

The gravity data shows a prominent positive anomaly in the necking zone.

The necking zone of the SL01 is partially constrained in the wide-angle data (Figures 8 and 15), but in the MCS (Figures 4 and 14), it presents a zone of intracrustal reflectors between 4 and 8 km depth and between 10 and 70 km model distance. We can recognize few SDRs pattern in this zone, and, in the GXT-ION profiles, a group of deeper reflectors in the lower crust, near the Moho discontinuity, between 20 and 25 km depth, and between 20 and 80 km model distance. These reflectors were interpreted by Mohriak *et al*. (1998) as a gradational passage from the lower crust to the lithospheric mantle. In this same zone, we observe a very irregular topography in the basement, showing some structures that look like volcanic plugs (Mohriak *et al.*, 1995, 1998).

This zone gives a chaotic response in the wide-angle data. Additionally, the fact that this area is a zone with poor data coverage and no inland continuation makes difficult a detailed interpretation of the crustal framework near the base of the crust. However, in wide-angle data, the Pmp is very clear and allows us to make a good interpretation of the Moho discontinuity. It rises from 25 km depth in the extreme NW of the profile to 18 km in the transition of the continental to oceanic crust at ~70 km distance in the profile (Figure 8). In the lower crust, the array of basal intra-crustal reflectors is disposed in an anticlinal pattern that gives an idea of a lenticular shape (figure 8). In this zone, the velocity goes from 7.0 to 7.3 km/s laterally. Loureiro *et al*. (2018) found some similar structures in the profile SL11, located at the Jequitinhonha basin, near a zone of “necking zone wideness” transition.

Buck (1991, 1999) reports “a series of basins and ranges in a broad region of continental extension”. According to Buck (1999), this pattern, is related to lateral periodic variations in the rate of extension, which causes the so-called "lithospheric *boudinage*". This process of *boudinage* of the lithosphere produces variations on the local isostasy, also called crustal buoyancy (Block and Royden, 1990; Bird, 1991; Buck, 1991, 1999).

From the Continental Domain to seawards, the total crustal thickness, without the water column (~4 km through the COB) and sediment cover, thins from ~33 km at the most continental part, to ~10 km through the COB and the change in the velocity of the lower crust may therefore be interpreted as a density compensation to effect of *boudinage* process and/or as volcanic intrusions.

ACCEPTED MANUSCRIPT

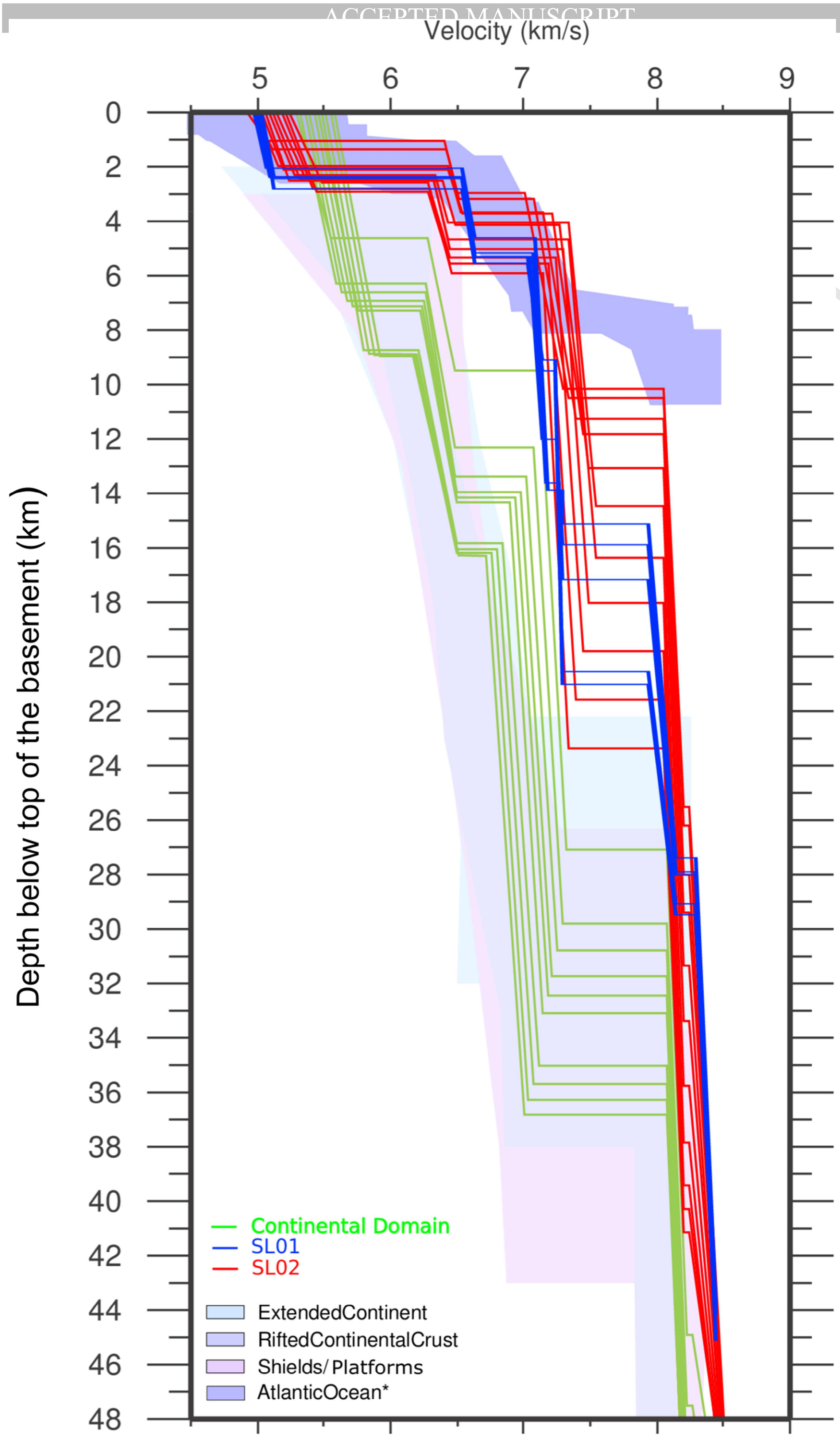
Velocity (km/s)
5
6
7
8
9
0
2
4
6
8
10
12
14
16
18
20
22
24
26
28
30
32
34
36
38
40
42
44
46
48
Depth below top of the basement (km)
Continental Domain
SL01
SL02
ExtendedContinent
RiftedContinentalCrust
Shields/Platforms
AtlanticOcean*

652

Figure 17: Compilation of 1D velocity-depth profiles extracted below the top of the basement (Vz) in the Unthinned Continental Domain (green lines) and the Necking Zone (red and blue lines). The blue shaded area bounds a compilation of velocity profiles for typical Atlantic oceanic crust (White et al., 1992), and light blue areas correspond to averaged velocity profiles for continental crust (Christensen and Mooney, 1995).

Figure 17 shows that the transition between the unthinned continental crust and the thinned domain preserves the configuration and the velocities of the crustal layers with strong velocity steps. The total crustal thickness has a sharp transition and the comparison of the Vz of the two profiles with the compilations for a typical continental crust (Christensen and Mooney, 1995) and for Atlantic-type oceanic crust (White *et al.*, 1992), shows that the crustal nature in the necking zone is closer to a typical continental crust than a typical oceanic crust (Figure 17). We propose that the necking seems therefore to be constituted by thinned continental crust, that presents a continuity of the velocity structure during the thinning process, without the presence of a transitional crust, and the main change to oceanic crust occurs outside the Necking Zone.

Oceanic domain:

The External Domains (25-210 km distance model on SL02 and 70-210 on SL01) show a thinner crustal thickness and is interpreted as formed by oceanic crust. The sedimentary cover is also thinner and reaches 3 km. The top of the basement located at 6-8 km depth assumes a much more regular topography. The crustal layers do not present any significant lateral velocity gradient through the transition from continental to oceanic crust. Figures 15 and 18 show that, except under the volcanic edifice, where the top of the basement follows the topography of the volcano, the average depth of the oceanic basement varies between 6 to 8 km (Figure 8).

Due to the fact that this crust was formed during the Cretaceous Normal Superchron (CNS), a magnetic quiet period, it presents a lack of reversal-related magnetic anomalies on crust of age 121 (Anomaly M0y) to 83.6 (Anomaly C34y) Ma old (Malinverno *et al.*, 2012; Ogg, 2012; Granot *et al.*, 2014).

Nevertheless, the Vz profiles (Figure 18) along the profiles SL01 and SL02 show that the oceanic basement and its layers fit almost perfectly the worldwide compilation for Atlantic-type oceanic crust (White *et al.*, 1992). The Moho has a range of depths below basement that varies from 6 to 12 km. It slightly rises from NW to SE in the proximal part of the oceanic domain (Figure 18), of the closest to the transition with continental crust, and deepens under the volcanic edifice along SL02 profile. The rest of the oceanic crust thickness ranges from 8 to 6 km (Figure 18). Larger Moho depths under the volcano can be justified due to the presence of the undercrustal layer that reflects isostasy compensation. Despite the thick crust in this area, crustal velocities go according with the compilation of a typical oceanic crust (White *et al.*, 1992).

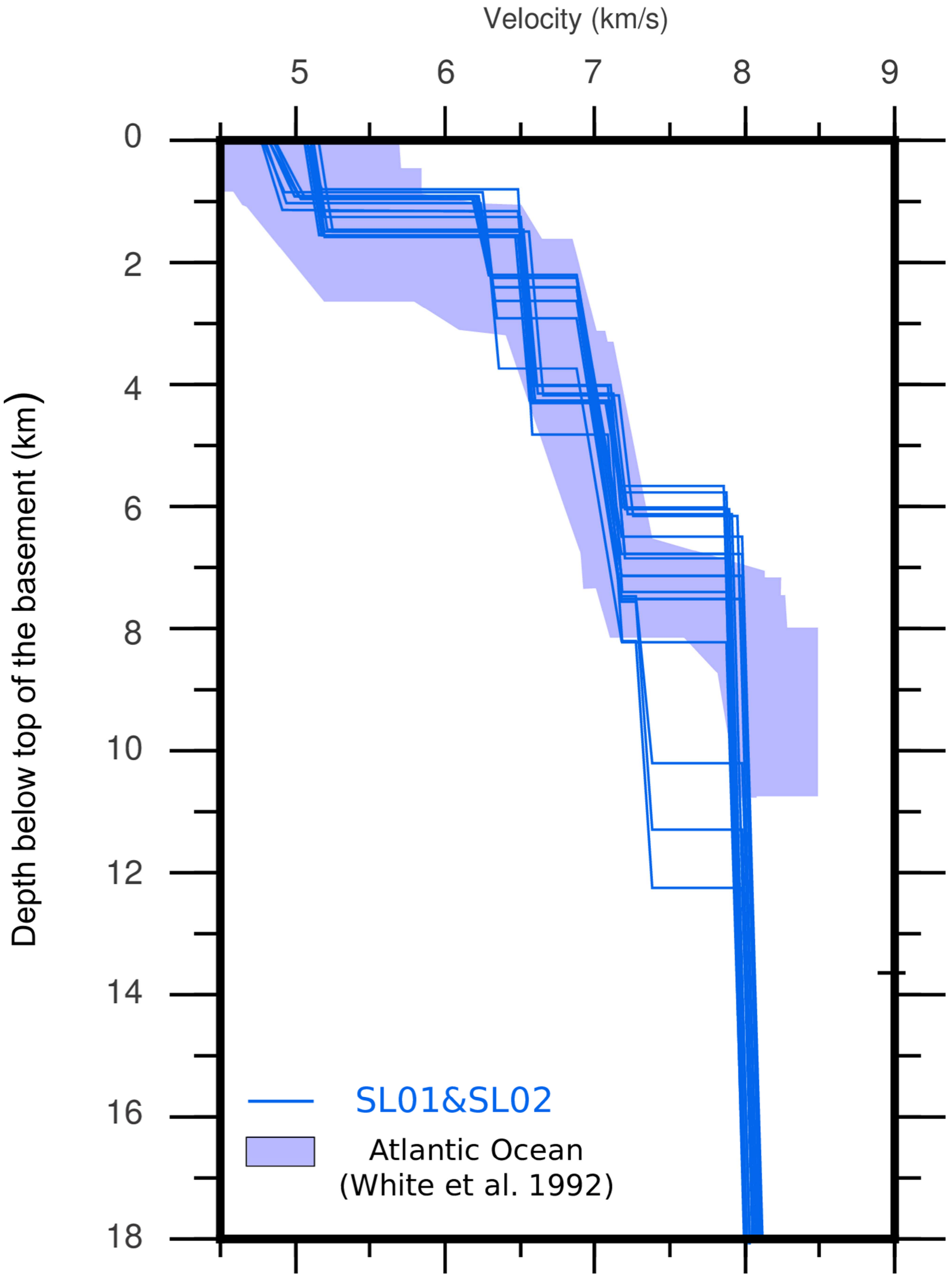
Velocity (km/s)
5
6
7
8
9
0
2
4
6
8
10
12
14
16
18
Depth below top of the basement (km)
SL01&SL02
Atlantic Ocean
(White et al. 1992)

Figure: 18 Compilation of 1D velocity-depth profiles extracted below the top of the basement (Vz) in the proposed Oceanic Crust. Colored lines mark individual Vz profiles at a 10 km interval of profiles SL01 and SL02. The blue shaded area bounds a compilation of velocity profiles for typical Atlantic oceanic crust (White et al., 1992).

The figure 8 shows a comparison between the data and the segmentation obtained in this work and a line-drawing of the ION-GXT seismic profiles. The wide-angle models go mostly in accord with the crustal structures interpreted from the ION-GXT lines, except for the Moho along SL01 which is modeled on average 2 km shallower with wide-angle data than the deepest reflector seen on the depth converted MCS line.

Continental-Oceanic Boundary

The transition between the continental and the oceanic domain is characterized in the MCS profiles (Figures 4 and 14) by a zone dominated by intracrustal reflectors. These reflectors in most part look like SDRs, but there is also some that are similar to LDRs. At this zone, the basement topography shows some mounds and little elevations. All these structures could be classified as a magmatic signature. Notwithstanding that, as Moulin *et al.* (2005) noticed already, these structures are not sufficient to characterize an archetype that could classify the margin of the SAB as a volcanic margin similar to the Greenland or Argentina Margins. Moreover, there is no evidence in the bibliography of volcanism before the first production of ocean crust. As described by Mohriak *et al*. (1998), these magmatic features are probably associated with extensional processes and oceanic crust inception, and they apparently post-date the rift phase lithospheric extension associated with the breakup of Gondwana in the Early Cretaceous, and were used by Mohriak *et al*. (1995, 1998) and Blaich *et al.* (2008) for their localization of the COB. Based on our wide-angle data analysis, we pointed the COB at ~70 km from the coast, between the SL02OBS13 and SL02OBS12 along the SL02 profile just seaward of the slight velocity increase in the lower crust, and ~100 km from the coast, between the SL01OBS05 and the SL01OBS06, along the SL01 profile just seaward of the intra-crustal velocity body, a little further seaward than the COB pointed by these authors.

Conclusions

The P-wave modelling of the SL01 and SL02 profiles reveals the deep crustal structure of the SAB passive margin off NE Brazil. From these models, we conclude that:

- The SAB margin is segmented parallel to the NE-SW coastline and the hinge line of the platform into a Continental Domain, a Necking Zone and an Oceanic Crust Domains without transitional domain.
- The oceanic crust is therefore rapidly reached, less than 100 km from the coast; its limit is parallel to the coast all along this segment. The COB is therefore situated a little further seaward than pointed out by Mohriak *et al*. (1995, 1998) and Blaich *et al*. (2008).
- These results show the huge segmentation in the offshore deep structures of the NE Brazilian margins since as opposed to this study a wide transitional domain of exhumed lower continental crust is imaged 350 km southwards in the Jequitinhonha margin (Loureiro *et al.*, 2018).
- Onshore, LSS data along SL02 profile allow the characterization of the unthinned continental crust. It is ~30–35 km thick, divided into three layers with velocities between 5.0 and 7.2 km/s. The results confirm the general trend modelled by previous studies of Mohriak *et al*. (1995, 1998); Blaich *et al*. (2008).
- The Necking Zone presents a rather sharp crustal thinning on the north of the Vaza-Barris fault (SL02), where the Moho goes from 31 km to 18 km depth in less than 100 km, and the first thinning corresponds to the vanishing of the upper crust, that thins from 10 km, at the continental domain, to less than 2 km through the COB, and keeps this thickness seawards. The Moho rises from a depth of 33 km at the limit with Continental Domain to a depth of 16 km through the COB. The lateral velocity variation happens only in the lower crust where it goes from 7.0 to 7.3 km/s at the top and from 7.25 to 7.5 km/s at the base. This wide-angle model shows a Moho located slightly (2 km) shallower than the one found by Mohriak *et al*. (1998) and confirms the gravity model of Blaich *et al*. (2008).
- Further SE, a 9 km thick typical oceanic crust is present, with a thin upper layer (1–1.5 km) that presents velocities varying from 5.0 to 5.20 km/s, a 2.5 km thick middle layer with velocities of 6.5–6.6 km/s, and a thicker lower layer with 3-4 km thick and 6.9 to 7.1 km/s. The transition between the necking zone and this domain is characterized by a zone dominated by intracrustal reflectors, which could reflect a magmatic signature, notwithstanding that, as Moulin *et al*. (2005) noticed already, these structures are not sufficient to characterize an archetype that could classify the margin of the SAB as a volcanic margin. As described by Mohriak *et al*. (1998), these magmatic features are associated with extensional processes and oceanic crust inception, and they apparently post-date the rift phase lithospheric extension associated with the breakup of Gondwana in the Early Cretaceous.

- This oceanic crust is affected on profile SL02 by a volcanic edifice with 40 km extension where the basement rises almost 4 km. The Bahia Seamounts chain has U/Pb ages from 75 to 84 Ma and is supposed to be related to a post-rift hotspot localized near the Middle Atlantic Ridge (MAR) (Skolotonev, 2012). Below this domain, there is a sub-crustal layer, very well constrained by the OBS and gravity data, with ~5 km thick and 7.3 km/s velocity. This layer is probably related to a magmatic underplating process where basaltic magmas are frequently trapped at or near the Moho, or within the crust, or in complex crust-mantle transition zones (Cox,1993).

- The undulated intracrustal reflectors, with an anticlinal shape, in the base of the lower crust of the necking zone in SL01 profile, added to the rise in the seismic velocity are a good evidence that the rift caused a lithospheric boudinage. This zone of boudinage is near of and is probably affected by the Vaza-Barris Transfer Zone. A similar feature is observed further in the south, at the Jequitinhonha Basin (Loureiro *et al.*, 2018), where the crust is also affected by boudinage, near a zone of “necking zone wideness” transition. Buck *et al.* (1999) proposed that lithospheric boudinage is formed under local isostatic effect, sometimes called crustal buoyancy. Due to a possible heterogeneity, the crust was affected by a non-homogeneous thinning and extension, generating crustal boudinage. It can be explained by some transformations in the composition of the lower crust under the necking. On the other hand, this boudinage could be a consequence of magmatic intrusions formed during the rift process. However, the Pmp in the wide-angle data, is clear and continuous, and do not seem to have been influenced by a volcanic intrusion.

- The SFB, which was in the margin of the Pernambuco Alagoas Domain, and was formed by thrust faulting of this domain over the São Francisco Craton during the Brasiliano orogeny, resulting in the collage of its crusts (Oliveira *et al.*, 2010). The comparison between velocity models of the Pernambuco Alagoas Domain (Soares *et al.*, 2010; Tavares *et al.*, 2012; de Lima *et al.*, 2015) and the São Francisco Domain (Soares *et al.*, 2006 and Soares, personal communication), shows that the crust in the SFB is much more similar to the Pernambuco Alagoas Domain than to the São Francisco Craton. This could mean that the São Francisco crust was subducted and consumed, and the crust of the Pernambuco-Alagoas predominated in the Brasiliano orogenic event as it was proposed by Oliveira *et al.* (2010).

Contributions

The SALSA Project was led by D. Aslanian and M. Moulin, from Ifremer, and A. Viana and J. A. Cupertino, from Petrobras. Modeling of the SALSA profile was done by M. Evain, A. Afilhado, F.

Gallais, A. Loureiro, F. Schnurle and F. Klingelhoefer. On-land operation was conducted by J. Soares, R. Fuck, M. Vinicius de Lima, from the University of Brasilia (UnB) L. Matias, and C. Corela from the Instituto Dom Luis (IDL) of the University of Lisbon. Processing of the MCS seismic data was done by P. Schnurle. This work has been conducted as part of a PhD project supported by the Conselho Nacional de Desenvolvimento Científico e Tecnológico (CNPQ) from Brazil.

Acknowledgments

The data set collected during the SALSA experiment is protected under a partnership between IFREMER and Petrobras. Any request has to be addressed to Daniel Aslanian (aslanian@ifremer.fr) and Adriano Viana (aviana@petrobras.com.br). The authors wish to thank the captain, crew, and MCS technical team of the French R/V L'Atalante. Many thanks also to the OBS and land station technical teams who made this experiment possible. The GMT [Wessel and Smith, 1998], Seismic Unix software package [Stockwell, 1999], GEOCLUSTER software (CGG-Veritas), and RAYINVR software (Zelt and Smith, 1992; Zelt *et al*., 1999) were used in the preparation of this paper. The Salsa Team is composed by: Morvan, L.[1]; Mazé, J.P.[1]; Pierre, D.[1]; Roudaut-Pitel, M.[1]; Rio, I.[3], Alves, D.[3]; Barros Junior, P.[7]; Biari, Y.[1]; Corela, C.[3]; Crozon, J.[1]; Duarte, J.L.[3]; Ducatel, C.[1]; Falcão, C.[7]; Fernagu, P.[1]; Le Piver, D.[1]; Mokeddem, Z.[6]; Pelleau, P.[1]; Rigoti, C.[7]; Roest, W.[1]; Roudaut, M.[1].

We would like to thank two anonymous reviewers and the editor Dr. F. Audemard, who helped to improve significantly this manuscript.

References

Almeida F. F. M., Hasui Y., Brito Neves B.B. Fuck R.A. (1977). Províncias Estruturais Brasileiras. *In*: SBG-Núcleo Nordeste, Simpósio Geologia do Nordeste, 8, Campina Grande, *Atas*, Boletim 6, p. 363-391.

Austin, J. A., Jr., and Uchupi, E. (1982). Continental-oceanic crustal transition of Southwest Africa. Am. Assoc. Petrol. Geol. Bull., 66, 1328±1347

Bauer, K., Neben, S., Schreckenberger, B., Emmermann, R., Hinz, K., Fechner, N., Gohl, K., Schulze, A., Trumbull, R. B., Weber, K. (2000). Deep structure of the Namibia continental margin as derived from integrated geophysical studies. *Journal of Geophysical Research: Solid Earth*, *105*(B11), 25829-25853.

Blaich, O.A., Tsikalas, F., Faleide, J.I. (2008). Northeastern Brazilian margin: regional tectonic evolution based on integrated analysis of seismic reflection and potential field data and modelling. Tectonophysics, 458: p.51-67.

Blaich, O.A., Faleide, J.I. Tsikalas, F. 2011. Crustal breakup and continent-ocean transition at South Atlantic conjugate margins. Journal of Geophysical Research, 116, B01402, doi:10.1029/2010JB007686.

Black, R., and Girod, M. (1970). Late Paleozoic to Recent igneous activity in West Africa and its relationship to basement structure. *African magmatism and tectonics*, *1*(8), 5-2.

Bonatti, E. (1996). Anomalous opening of the Equatorial Atlantic due to an equatorial mantle thermal minimum. *Earth and Planetary Science Letters*, 143: 147-170.

Buck, W. R., Lavier, L. L., Poliakov, A. N. (1999). How to make a rift wide. *Philosophical Transactions-Royal Society of London Series a Mathematical Physical and Engineering Sciences*, 671-689.

Cainelli, C. (1992). Sequence stratigraphy, canyons, and gravity mass flow deposits in the Piacabuçu Formation, Sergipe-Alagoas Basin, *Brasil. PhD thesis, University of Texas at Austin*, 233 p.

Cainelli, C., and Mohriak, W. U. (1998, November). Geology of Atlantic eastern Brazilian basins. In *Brazilian Geology Part* (Vol. 2, p. 1998).

Carvalho, M. J., (2005). Tectonic Evolution of the Marancó-Poço Redondo Domain: Records of the Cariris Velhos and Brasiliano Orogenesis in the Sergipano Belt, NE Brazil. Tese de doutorado. Universidade de Campinas.

Campos Neto, O., Lima, W. S., Cruz, F. G. (2007). Bacia de Sergipe-Alagoas. *Boletim de Geociências da PETROBRAS*, *15*(2), 405-415.

Christensen, N. I., and Mooney, W. D. (1995). Seismic velocity structure and composition of the continental crust: A global view. *Journal of Geophysical Research: Solid Earth*, *100*(B6), 9761-9788. doi:10.1029/95JB00259

Cohen, J. K. and Stockwell Jr., J. W. (2010). CWP/SU: Seismic Unix Release 42: a free package for seismic research and processing, *Center for Wave Phenomena, Colorado School of Mines.*

Cornacchia, M., and Dars, R. (1983). Un trait structural majeur du continent Africain; les lineaments centrafricains du Cameroun au Golfe d'Aden. *Bulletin de la Société Géologique de France*, *7*(1), 101-109.

Conceição, J.C.J., Zalán, P.V., Wolff, S. 1988. Mecanismo, Evolução e Cronologia do Rift Sul-Atlântico, Boletim de Geociências da PETROBRAS, 2(4):255-265

Contrucci, I., Matias, L., Moulin, M., Géli, L., Klingelhofer, F., Nouzé, H., Aslanian D., Olivet J. L., Réhault J. P., Sibuet, J. C. (2004). Deep structure of the West African continental margin (Congo, Zaïre, Angola), between 5 S and 8 S, from reflection/refraction seismics and gravity data. *Geophysical Journal International*, *158*(2), 529-553.

Davison, I. and Santos, R.A., (1989). Tectonic evolution of the Sergipano Fold Belt, NE Brazil, during the Brasiliano Orogeny. Precamb. Res., 45. p. 319-342.

D’el-Rey Silva, L. J. H. (1999). Basin infilling in the southern-central part of the Sergipano Belt (NE Brazil) and implications for the evolution of Pan-African/Brasiliano cratons and Neoproterozoic sedimentary cover. *South American Journal of Earth Sciences*, *12*: 453-470

Dumont, J. F. (1986). Identification par télédétection de l'accident de la Sanaga (Cameroun): Sa position dans le contexte des grands accidents d'Afrique Centrale et de la limite nord du craton Congolais. *Géodynamique*, *1*(1), 13-19.

Eldholm, O., Thiede J., and Taylor E. (1989). Evolution of the Vøring volcanic margin, *Proceedings of the Ocean Drilling Program - Scientific Results*, 104, 1033-1065.

Feijó, F. J. (1994). Bacia de Sergipe–Alagoas. Boletim de Geociências da PETROBRAS, Rio de Janeiro, 8(1):149-161

Gomes, P. O. (2005). Tectonismo, Vulcanismo, Sedimentação e Processos erosivos No Segmento Nordeste Da Margem Continental Brasileira. *Phd thesis. Universidade Do Estado Do Rio De Janeiro Faculdade De Geologia*.

Humphrey, F. L.; Allard, G. O. (1969). Geologia da área do domo de Itabaiana (SE) e sua relação com a geologia do geossinclinal de Propriá – Um elemento tectônico recem-conhecido no Escudo Brasileiro. (1969). *Tradução de Munne, A. I., Barão, S. C. Rio de Janeiro, PETROBRAS/CENPES*, 157 p. il.: mapa.

Klemperer, S. L., Hauge, T. A., Hauser, E. C., Oliver, J. E., Potter, C. J. (1986). The Moho in the northern Basin and Range province, Nevada, along the COCORP 40 N seismic-reflection transect. *Geological Society of America Bulletin*, *97*(5), 603-618.

Korenaga, J., Holbrook, W. S., Kent, G. M., Kelemen, P. B., Detrick, R. S., Larsen, H. C., Dahl-Jensen, T. (2000). Crustal structure of the southeast Greenland margin from joint refraction and reflection seismic tomography. *Journal of Geophysical Research: Solid Earth*, *105*(B9), 21591-21614.

Lana, M. C. (1990) Bacia de Sergipe-Alagoas: Uma Hipótese de Evolução Tectono-Sedimentar. *Origem e Evolução de Bacias Sedimentares - coordenadores Raja Gabaglia, G. P. e Milani, E. M - Petrobras/Serec/Censud*, p.311-332.

de Lima, M. V. A., Berrocal, J., Soares, J. E., Fuck, R. A. (2015). Deep seismic refraction experiment in northeast Brazil: New constraints for Borborema province evolution. *Journal of South American Earth Sciences*, *58*, 335-349.

Liu, Z., Bleistein, N. (1995). Migration velocity analysis: Theory and an iterative algorithm. *Geophysics*, *60*(1), 142-153.

Ludwig W.J., Nafe J.E. Drake L.E. (1970). Seismic refraction. Maxwell, A.E. (Editor), *The Sea. New concepts of sea floor evolution*. Wiley-Interscience, New York, 4(I): 53-84.

Lutter, W. J., Nowack, R. (1990). Inversion for crustal structure using reflections from the PASSCAL Ouachita experiment. *Journal of Geophysical Research: Solid Earth*, *95*(B4), 4633-4646.

Mohriak, W.U., Rabelo, J.H.L., Matos, R.D., Barros, M.C. (1995). Deep Seismic Reflection Profiling of Sedimentary Basins offshore Brazil: Geological Objectives and Preliminary Results in the Sergipe Basin. *Journal of Geodynamics, 20:*515-539

Mohriak, W.U., Bassetto, M. Vieira, I.S. (1998). Crustal Architecture and Tectonic Evolution of the Sergipe–Alagoas and Jacuípe Basins, Offshore Northeastern Brazil. *Tectonophysics, 288*:199-220.

Mohriak, W.U., Mello, M.R., Bassetto, M., Vieira, I.S., Koutsoukos, E.A.M. (2000). Crustal architecture, sedimentation, and petroleum systems in the Sergipe–Alagoas Basin, Northeastern Brazil. *In*: Mello, M.R., Katz, B.J. (eds.). *Petroleum systems of South Atlantic margins, AAPG Memoir 73:*273-300

Mohriak, W. U. (2003). Bacias sedimentares da margem continental Brasileira. *Geologia, tectônica e recursos minerais do Brasil*, *3*, 87e165.

Moulin, M., D. Aslanian, J.-L. Olivet, I. Contrucci, L. Matias, L. Géli, F. Klingelhoefer, H. Nouzé, J.-P. Réhault, and P. Unternehr (2005). Geological constraints on the evolution of the Angolan margin based on reflection and refraction seismic data (ZaïAngo project). *Geophysical Journal International*, *162*(3), 793-810.

Moulin, M., D. Aslanian, and P. Unternehr (2010), (2010). A new starting point for the South and Equatorial Atlantic Ocean. *Earth-Science Reviews*, *98*(1-2), 1-37.

Oliveira, D.C., Windley, B.F., Araújo, D.B. (2010). The Neoproterozoic Sergipano orogenic belt, NE Brazil: A complete plate tectonic cycle in western Gondwana. *Precambrian Research 181*, 64-84.

Oliveira, R. G. D. (2008). Arcabouço geofísico, isostasia e causas do magmatismo cenozóico da Província Borborema e de sua margem continental (Nordeste do Brasil).

Pavlis, N. K., Holmes, S. A., Kenyon, S. C., Factor, J. K. (2012). The development and evaluation of the Earth Gravitational Model 2008 (EGM2008). *Journal of Geophysical Research: Solid Earth*, *117*(B4).

Sandwell, D. T., Müller, R. D., Smith, W. H., Garcia, E., Francis, R. (2014). New global marine gravity model from CryoSat-2 and Jason-1 reveals buried tectonic structure. *Science*, *346*(6205), 65-67.

Sandwell, D., Smith, W. (1997). Marine gravity anomaly from GEOSAT and ERS-1 satellite altimetry. *Journal of Geophysical Research, 102:10.039*-10.054.

Santos, E. D., Silva Filho, M. A. (1975). Ensaio interpretativo sobre as evolução da Geossinclinal de Propriá, Nordeste do Brasil. *Revista Mineração e Metalurgia*, *367*, 3-22.

Schaller, H. (1970). Revisão estratigráfica da bacia Sergipe-Alagoas. Boletim Técnico da Petrobrás. 12 (1): 21-86

Skolotnev S. G., Bylinskaya M. E, Golovina L. A., and Ipat'eva I. S. (2012). The Origin of Bahia Seamounts (Brazil Basin, South Atlantic) in Connection to New Data on Their Age. *Doklady Earth Sciences, 2012, Vol. 443, Part 2, pp. 444–450. ISSN 1028_334X.*

Silva Filho, M. A., (1998). Arco vulcânico Canindé-Marancó e a Faixa Sul-Alagoana: sequências orogênicas Mesoproterozóicas. In: XL *Congresso Brasileiro de Geologia, Belo horizonte, SBG.* p. 16.

Soares J.E.P., Berrocal J., Fuck R.A., Mooney W.D. Ventura D.B.R. (2006). Seismic characteristics of central Brazil crust and upper mantle: A deep seismic refraction study. *Journal of Geophysical Research*, 111: 1-31.

Soares, J. E. P., de Lima, M. V., Fuck, R. A., Berrocal, J. (2010). Características sísmicas da litosfera da Província Borborema: Resultados parciais do experimento de refração sísmica profunda. In *IV Simpósio Brasileiro de Geofísica*.

Stockwell, J. W., Jr. (1999), The CWP/SU: Seismic Un x package, Comput. Geosci., 25(4), 415–419, doi:10.1016/S0098-3004(98)00145-9.

Szatmari, P. (1998). Tectonic habitat of petroleum along the South Atlantic margins. In Am. Assoc. Petrol. Geol. *International Conference Extended Abstracts Volume, Rio de Janeiro, Brazil,* pp. 362±363.

Szatmari, P., Milani, E.J. (1999). Microplate rotation in northeast Brazil during South Atlantic rifting: analogies with the Sinai microplate. Geology, 27(12):1115-1118

Tard F., Masse P., Walgenwitz F., Gruneisen P., The volcanic passive margin in the vicinity of Aden, Yemen, Bulletin des centres de recherche et d'exploration-production Elf-Aquitaine 15 (1991) 1–9

Tavares, E. J., Soares, J. E. P., Fuck, R. A., De Lima, M. V. A. (2012). Modelagem de onda P e razão Vp/Vs da crosta sob a linha de refração sísmica profunda NW-SE da Província Borborema. In *V Simpósio Brasileiro de Geofísica*.

White, R. S., McKenzie, D. and O'Nions, R. K. (1992). Oceanic crustal thickness from seismic measurements and rare earth element inversions. *Journal of Geophysical Research: Solid Earth*, *97*(B13), 19683-19715. doi:10.1029/92JB01749.

Zelt, C. A. (1999), Modelling strategies and model assessment for wide angle seismic traveltime data, *Geophysical Journal International*, *139*, 183–204.